Study of Pressure Effects on Quasi-One-Dimensional Molecule-Based Magnets

Kentaro Suzuki

DOCTOR OF PHILOSHPHY

Department of Structural Molecular Science

School of Mathematical and Physical Science

The Graduate University for Advanced Studies

2002

Contents

# 1. Introduction

Introduction

Since 1980's, the molecule-based magnets of the coordination polymers organic radicals and transition metals, has been studied.[1-4] Several of them have been established to have finite critical temperatures for undergoing transitions to ferro- and/or ferrimagnets.[4, 5] A large number of molecule-based magnets have been prepared and reported.[1-23]

A characteristic feature of this type of the molecule-based magnets is self-assembling of metals and organic radical molecules. Organic radical parts can be modified by techniques of organic syntheses. Strong magnetic interactions between radicals and transition metals are expected. The dimensionality of this type of the molecule-based magnets is controllable; one-,[1-13] two-[12, 14-19] and three-dimensional networks[20-23] have been constructed, depending on the shapes of radicals and coordinations of metals.

Magnetic ordering of low dimensional magnets requires some additional interchain and/or interlayer interactions. Interchain or interlayer interactions play an important role in the magnetic behavior around the transition temperatures.[23] One-dimensional molecule-based magnets include a chain structure formed by the coordination bonding of metal and radical. Between chains, van der Waals forces exist. Weak interchain interactions sometimes cause three-dimension magnetic phase transitions. When we change the substituents of the organic radical, the interchain packings are often modified, but the chain structures made of the coordinating bonds are less affected.

In this thesis, the pressure effects on the magnetic properties of the

one-dimensional chain complexes of Mn(hfac)$_2$ (hfac = hexafluoroacethylacetonate) with 1,3-bis(*N-tert*-butylamionoxyl)benzene (BNO) or its 5-halogeno derivatives (X-BNO's; X = F, Cl and Br)) (abbreviated as [Mn(hfac)$_2$]·(BNO) or [Mn(hfac)$_2$]·(X-BNO), respectively),[11-13, 23d] were studied.
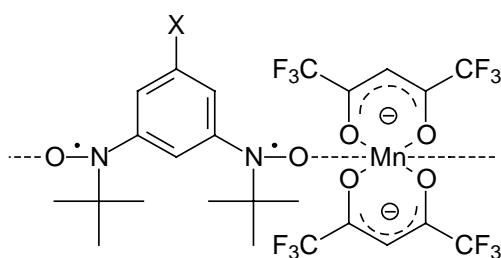
[Mn(hfac)$_2$]·(BNO) (X = H) and [Mn(hfac)$_2$]·(X-BNO) (X = F, Cl and Br)

These complexes construct a one-dimensional molecular chain composed of alternating alignment of Mn(hfac)$_2$ and BNO's. In spite of the different substituent of halogen atom, they form similar chain structures one another. The magnetic structure of the one-dimensional chain is ferrimagnetic, in which two different spins of $S = 1$ (BNO's radical) and 5/2 (Mn^{2+} ion) are coupled antiferromagnetically. At low temperatures, the four complexes undergo magnetic phase transitions due to weak interchain interactions.

[Mn(hfac)$_2$]·(BNO) and [Mn(hfac)$_2$]·(F-BNO) are metamagnets (T_N = 5.5 and 5.3 K, respectively), whereas [Mn(hfac)$_2$]·(Cl-BNO) and [Mn(hfac)$_2$]·(Br-BNO) are ferrimagnets (T_C = 4.8 and 5.3 K, respectively). The different ground states come from the different sign of the interchain interactions. The magnitude of the interchain interaction is estimated to be *ca.* 1000 times as small as that of the intrachain interactions.[13] The family of [Mn(hfac)$_2$]·(BNO) are a quasi-one-dimensional magnets.

The different interchain interactions are caused by the difference of the relative arrangements of the ferrimagnetic chains with the different halogen atoms. The pressurization is a good approach to obtaining the information about the interchain interactions of the complexes, because the chain arrangements are modified by pressure. The intrachain structures are very rigid because of the strong coordination bonds between the Mn atoms and BNO's radicals. The pressure effects on the intrachain structures are considered to negligible.

The some experimental results of the pressure effects on genuine organic radicals are listed in Table 1-1. In the cases of (4) and (5), the antiferromagnetic interactions are monotonously enhanced by pressure, while the antiferromagnetic interaction is reduced in (6). In the case of (1), the ferromagnetism is transformed into the antiferromagnetism by pressure. The high pressure can modify the intermolecular interactions of the genuine organic complexes through the modifications of the molecular packings.

Table 1-1 Example of the magnetic studies under pressure of genuine organic radicals[7]

(1) p-NPNN (β-phase) (Ferromagnet with T_C = 0.61 K) (Ref. 24)
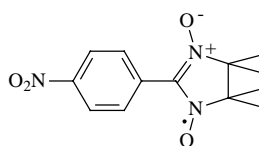
The ferromagnetic behavior is reduced with increasing pressure, and turns to antiferromagnetic above p = 6.5 kbar.

Table 1-1 (continued)

---

(2) *p*-Cl-ph-CH=N-TEMPO (Ferromagnet with T_C = 0.28 K) (Ref. 25)

   The pressure dependence of the magnetic behavior is shows the oscillation behavior; with increasing pressure, the ferromagnetic behavior is reduced up to 2.5 kbar, and enhanced up to 4.0 kbar. Such turning-point pres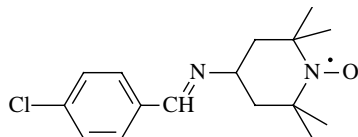sures are at 5.5, 7.5 and 9.0 kbar. Above 9.0 kbar, the ferromagnetic behavior is slightly enhanced with increasing pressure.

(3) Galvinoxyl (The structural phase transition is observed at 85 K) (Ref. 26)
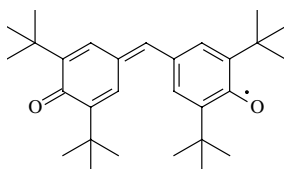
   The structural phase transition is inhibited by pressure.

(4) TPV and TOV (Antiferromagnet (weak Ferromagnet), T_N = 1.78 and 5.5 K, respectively) (Ref. 27, 28)
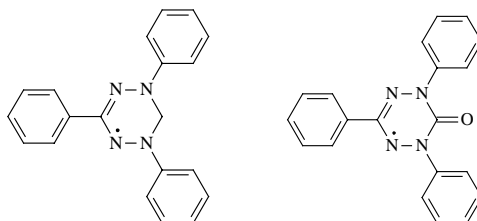
   The interchain interaction is monotonously enhanced with increasing pressure.

(5) TANOL and *p*-Cl-BDPA (Antiferromagnet) (Ref. 29, 30)
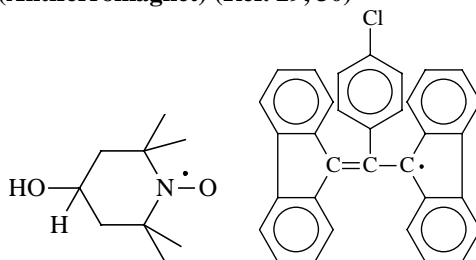
   The interchain interaction is monotonously enhanced with increasing pressure.

(6) F$_2$PNNNO (Antiferromagnet) (Ref. 31)
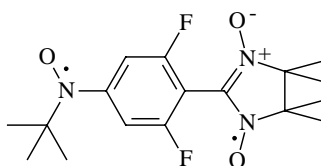
The antiferromagnetic interaction is reduced by pressure.

The magnetic behavior of the genuine organic magnets is very sensitive to the crystal packings, and their crystal structures are seriously affected by the difference of the molecular structures. Therefore, it is hand to carry out a systematic study on them, charging molecular packings finely. In our case, all the complexes have similar chain structures. By a systematic study on the m with making reference to one another, we can get insight into the magneto-structural correlations and the mechanisms of the magnetic exchange interactions in the metal-organic radical hybrid magnets.

References

1)   (a) A. Bencini, C. benelli, D. Gatteschi and C Zanchini, *J. Am. Chem. Soc., 106* (**1984**), 5813-5818, (b) C. Benelli, D. Gateschi, D. W. Carnrgie, Jr. and R. L. Carlin, *J. Am. Chem. Soc., 107* (**1985**) 2560-5561. (c) J. Laigier, p. Rey, C. Benelli, D. Gatteschi and C. Zanchini, *J. Am. Chem. Soc., 108* (**1986**) 6931.

2)   A. Caneschi, D. Gatteschi, J. Laugier and P. Rey, *J. Am. Chem. Soc., 109* (**1987**) 2191-2192.

3)   C. Benelli, A. Caneschi, D. Gatteschi, J. Laugier and P. Rey, in *Organic and Inorganic Low Dimensional Crysalline Materials* Ed By P. Delhaes and M. Drillon, Plenum, New York (**1987**)

4)   A. Caneschi, D. Gatteschi and R. Sessoli, *Acc. Chem. Res., 22* (**1989**), 292-398.

5)   A. Caneschi, D. Gstteschi, P. Rey, R. Sessoli, *Inorg. Chem., 27* (**1988**) 1756.

6)   A. Caneschi, D. Gateschi, J. P. Renard and P. Rey, *Inorg. Chem., 28* (**1989**) 2940.

7)   C. Benelli, A. Caneschi, D. Gatteschi, L. Pardi and P. Rey, Inorg *Chem., 28*(**1989**) 275.

8)   A. Chaneschi, D. Gatteschi, J. P. Rennarard, P. Rey and R. Sessoli, *J. Am. Chem. Soc., 111* (**1989**) 785.

9)   A Caneschi, D. Gatteschi, J. P. renard, P. Rey and R. Sessoli, *Inorg Chem., 28* (**1989**) 1976-1980.

10)   A. Caneschi, D. Gatteschi, J. P. Renard, P. Rey and R. Sessoli, *Inorg. Chem., 28* (**1989**) 3314.

11)   K. Inoue and H. Iwamura, *J. Chem. Soc. Chem. Commun.*, (**1994**) 2273-2274, (b) K. Inoue, T. Hayamizu and H. Iwamura., *Chem. Lett.* (**1995**) 745-746.

12)   (a) K. Inoue and H. Iwamura, *Synth. Met.*, 71 (**1995**) 1791-1794, (b) K. Inoue, T. Hayamizu and H. Iwamura, *Mol. Cryst. Liq. Cryst.*, 273 (**1995**) 67-80,

13)   (a) A. S. Markosyan, H. Iwamura and K. Inoue, *Mol. Cryst. Liq. Cryst.*, 334 (**1999**) 549 (b) K. Inoue, F. Iwahori, A. S. Markosyan, Y. Hosokoshi and H. Iwamura, *Coord. Chem. Rev. 198* (**2000**) 219.

14)   A. Caneschi, D. Gatteschi, M. C. Melandri, P. Rey and R. Sessoli, *Inorg. Chem., 29* (1990) 4228

15)   V. I. Ovchrenko, S. V. Larinov, K. E. Vostrikova, A. B. Burdukov, G. V. Romanenko, N. V. Pervuknina and N.V. Podberezeskaya, *Izv. Sib. Otd. Akas. Nauk S. S. S. R., Ser. Khim. Nauk., 5* (**1990**) 100

16) N. V. Pervuknina,V. L. Ikorskii, N.V. Podberezeskaya, P. S. Nikitin, A. B. Gel'man, V. I. Ovchrenko, S. V. Larinov and V. V. Bakakin, zh. Strukt. Khim 27 (**1986**) 61.

17) K. Inoue and H. Iwamura, *J. Am. Chem. Soc., 116*(**1994**) 3173-3174.

18) K. Inoue and H. Iwamura, *Adv. Mater, 8* (**1996**) 73-76

19) S. Hayami and K. Inoue, *Chem. Lett.* (**1999**) 545-549.

20) A. Caneschi, D. Gatteschi, J. P. Renard, P. Rey and R. Sessoli, *J. Am. Chem. Soc., 111* (**1989**), 785-786.

21) H. O. Stumpf, L. Ouahab, Y. Pei, D. Grandjean and O. Kahn, *Science, 231* (**1993**) 447-449.

22) K. Inoue, T. Hayamizu, H. Iwamura, D. Hashizume and Y. Ohahi, *J. Am. Chem. Soc.*, 118 (**1996**) 1803-1804.

23) (a) D. Gatteschi, O. Kahn, J. S. Miller and F. Paracio, Eds., *Magnetic Molecular Materials*, NATO ARI Series E, Kluwer Academic Publication (**1991**) E198, (b) J. S. Miller and A. J. Epstein, in *MOLLECULE-BASED MAGNETIC MATERIALS Theory, Techniques, and Apprication* Ed. by M. M. Thrnbull, T. Sugimoto and L. K. Thompson, ACS Symposium Series 644 (**1996**), p. 1. (d) H. Iwamura and K. Inoue, in *Magnetism: Molecules to Materials II* Ed. by J. S. Miller and M. D. Drillon, Wiley-VCH, Weinheim (**2001**) p. 61.

24) (a) K. Takeda., M. Mito, T. kawae, M. Takumi, K. Nagata, M. Tamura and M. Kinoshita, *J. Phys. Chem. B102* (**1999**) 671-676. (b) K. Takeda, M. Mito, T. Kawae, H. Deguchi, S. Takagi, M. Okumura, T. Kawakami, K. Yamaguchi and M. Kinoshita, *Chem. Phys., Lett.*, *308* (**1999**) 181-186.

25) M. Mito, T. Kawae, M. Hitaka, K. Takeda, T. Ishida and T. Nogami, *Chem. Phys. Lett., 333* (**2001**) 69-75.

26) Y. Hosokoshi, M. Tamura and M. Kinoshita, *Mol. Cryst. Liq. Cryst., 306* (**1997**) 423-430.

27) J. Yamauchi, K. Takeda and K. Konishi, *Mol. Cryst. Liq. Cryst., 233* (**1993**) 97-104.

28) M. Mito, M. Hitaka, T. Kawae, K. Takeda, K. Suzuki and K. Mukai, *Mol. Cryst. Liq. Cryst., 334* (**1999**) 369-378.

29) K. Takeda, N. Uryu, M. Inoue and J. Yamaguchi, *J. Phys. Soc. Jpn., 56* (**1987**) 736

30) J. Yamaguchi, K. Takeda and M. Inoue, *Chem. Lett.*, (**1990**) 1551.

31) Y. Hosokoshi and K. Inoue, *Syn. Metals*, 103 (**1999**) 2323

2. Experimental

2-1. Sample Preparation

The four complexes of $[Mn(hfac)_2]\cdot(BNO)$ and $[Mn(hfac)_2]\cdot(X\text{-}BNO)$ (X = F, Cl and Br) for the magnetic measurements were prepared following the method described in the literature.[1] A dichloromethane solution of BNO or X-BNO was added to a suspension of 1 equi-molar $Mn(hfac)_2$ in n-heptane. The mixture was concentrated under reduced pressure until black microcrystals of the complex precipitate. The microcrystals were removed by filtration and washed by n-hexane. The purities of samples were checked by magnetic measurements.

2-2. Magnetic Measurements

The measurement of dc magnetization (M) above 1.8 K was performed with the Quantum Design MPMS-2, -5S and -7 SQUID magnetometers. The measurement of ac magnetic susceptibility (χ_{ac}) above 2.0 K was performed with the Quantum Design MPMS-2 SQUID magnetometer, using the ac-field (H_{ac}) up to 5 Oe and the frequency (f_{ac}) up to 1 kHz. The typical condition of the measurements was H_{ac} = 5 Oe and f_{ac} = 1 Hz. The χ_{ac} at 1 Hz corresponds to the static magnetic susceptibility (χ_{dc}). The absolute value of χ_{ac} was obtained by the normalization of the data to fit the value of the χ_{dc} in the paramagnetic region.

2-3. High Pressure Cell

2-3-1. Design and Pressure Calibration

The dc magnetization and ac magnetic susceptibility under hydrostatic pressure were measured by using a high presser clamp cell made of Ti-Cu alloy.[2] A cross-sectional view of the cell is given in Figure 2-3-1. We used three cells with inner diameters of $\phi = 2.0$, 3.0 and 4.0 mm in the pressure regions of 4 ~ 12, 2.0 ~ 7.0 and 1.0 ~ 3.5 kbar, respectively.
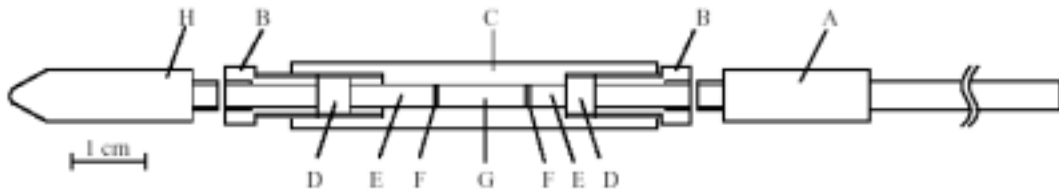
Figure 2-3-1 Cross-section view of the pressure clamp cell. A: Dummy cell (Connected to a sample rod), B: Locking nut, C: Cylinder, D: Backing plate (ZrO_2), E: Piston (ZrO_2), F: Cu seal, G: Teflon bucket, H: Dummy cell.

The samples (5 ~ 60 mg) were mounted with fomblin oil (H-VAC 140/13) as pressure transmitting medium in a Teflon bucket. The inner space of the Teflon cell is 10 mm length and the inner diameters of $\phi 1.5$, $\phi 2.4$ and $\phi 3.2$ for the outer diameters of $\phi 2$, $\phi 3$ and $\phi 4$, respectively. The actual pressure at low temperature is determined by the superconducting transition temperature of Pb[3] in the separate measurement. The relations between the actual pressure at around liquid [4]He temperature and load applied

at room temperature of three pressure clamp cells are shown in Figure 2-3-2.
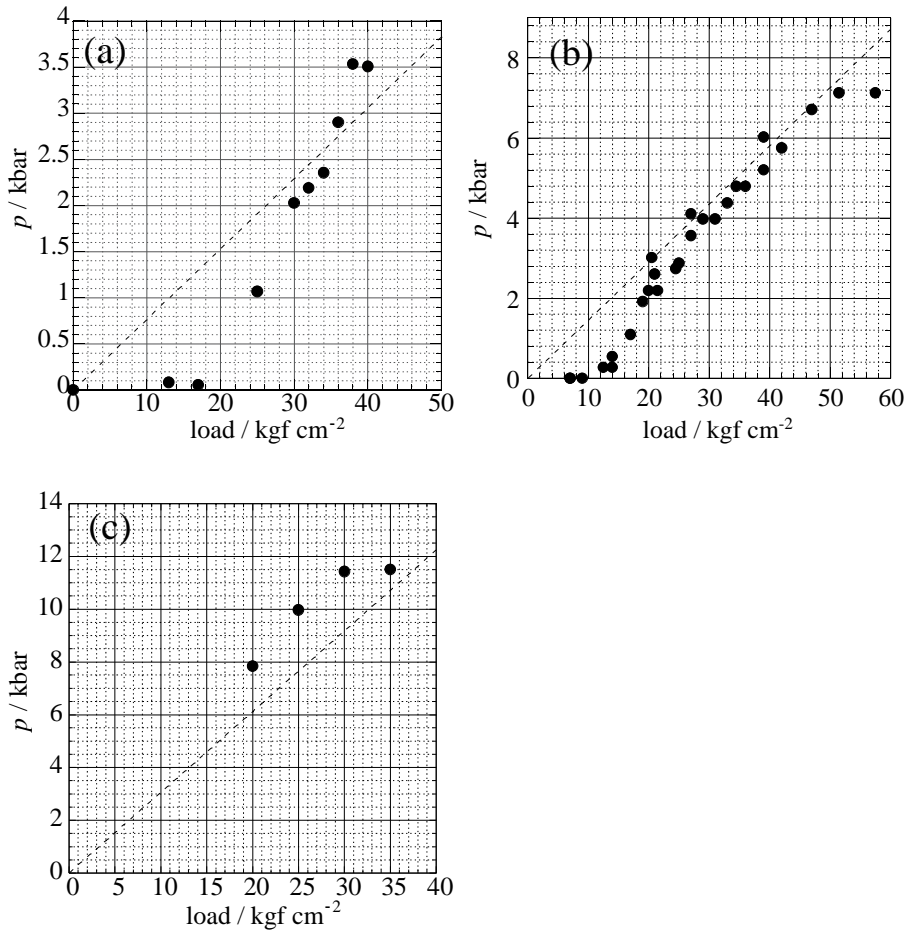
**Figure 2-3-2** Relation between the actual pressure at liquid ^{4}He temperature and the load applied at room temperature. The inner diameter of the cylinder is (a) $\phi 4$, (b) $\phi 3$ and (c) $\phi 2$. The dashed line is represents the relation simply estimated from the load and piston diameters.

2-3-2. Effect of High Frequency in the ac Magnetic Susceptibility Measurements

In the measurements of χ_{ac}, we must take care of the effect on eddy current on the metal surface of the pressure clamp cell. In order to minimize the effect of eddy current, it is preferable to use a low frequency for the measurements of χ_{ac}. As an

example, χ_{dc} and χ_{ac} of [Mn(hfac)$_2$]·(BNO) mounted in a capsule and a pressure-cell, are measured at 1 Hz compared and the results are shown in Figure 2-3-3. In the measurement using a clamp cell, the peak is slightly broadened but the peak appears at the same temperature as that seen in the capsule measurement.
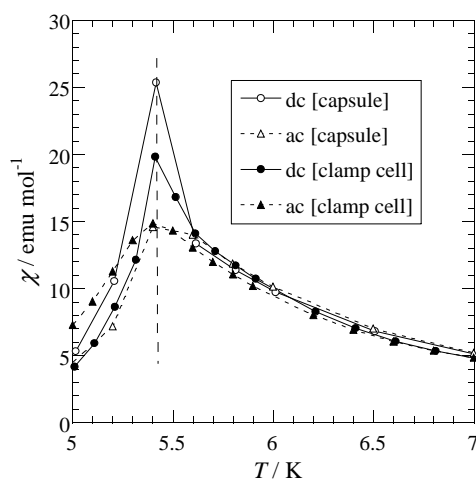

Figure 2-3-3 The comparison of the magnetic susceptibility measured in the ac or dc method. [Mn(hfac)$_2$]·(BNO) is mounted in a capsule, or in a Teflon bucket with oil to set a pressure clamp cell without compression.

In the measurement using the frequency up to 10 Hz, the effect of eddy current is negligibly small. Figure 2-3-4 shows the frequency dependence of χ_{ac}. The real and imaginably component is represented as χ' and χ'', respectively. The value of χ_{ac} of pressure clamp cell is temperature independent irrespective of frequency, as is shown in Figure 2-3-5. The observed data of χ_{ac} measured at a higher frequency than 10 Hz, were corrected by the subtraction of a constant value.
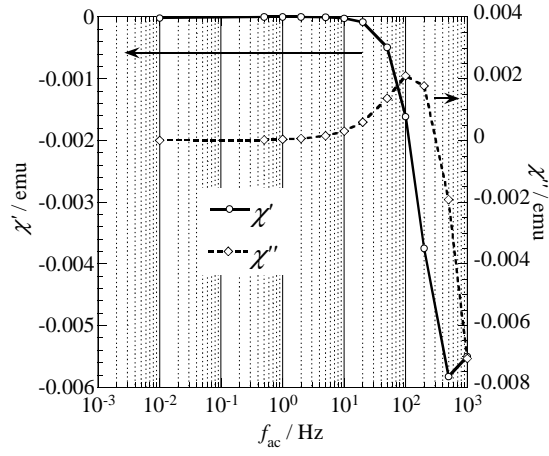
Figure 2-3-4. Frequency dependence of χ_{ac} measured at 10 K using a pressure cell without sample.
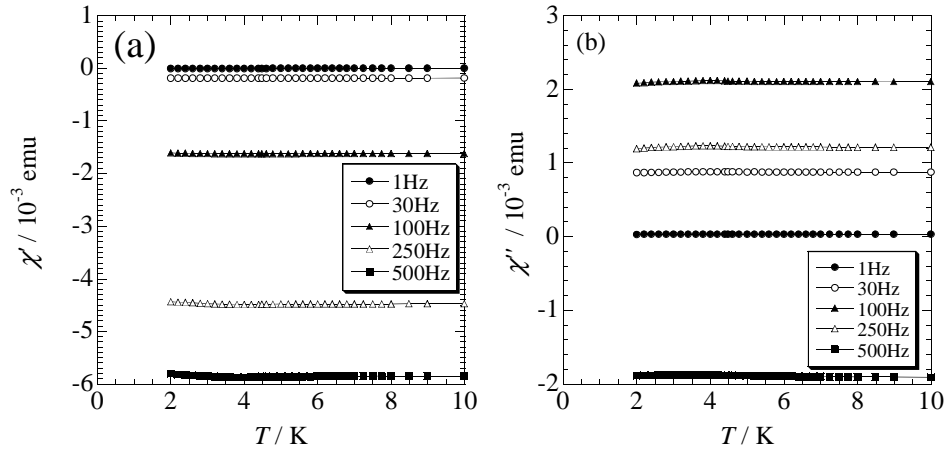
Figure 2-3-5. Temperature dependence of χ_{ac} of a high pressure cell measured at the several ac frequencies.

References

1) (a) K. Inoue and H. Iwamura, *J. Chem. Soc. Chem. Comm.*, (**1994**) 2272., (b) K. Inoue, F. Iwahori, A. S. Markosyan and H. Iwamura., *Coord., Cemistry Rev.*, 198 (**2000**) 219, (c) Iwamura and K. Inoue, in *Magnetism: Molecules to Materials II* Ed. by J. S. miller and M. D. Drillon, Wiley-VCH, Weinheim (**2001**), p 61.

2) Y. Hosokoshi, M. Tamura and M. Kinoshita, *Mol. Cryst. Liq. Cryst.*, 306 (**1997**) 423, Y. Hosokoshi, M. Mito, M. Tamura, K. Takada, K. Inoue, M. Kinoshita, *Rev. High Pressure Sci. Technol.* 1 (**1998**) 620.

3) A. Eiling and J. S. Schilling, *J. Phys. F*, 11 (**1981**) 623

3. Crystal Structures and Magnetic Properties of the Complexes at Ambient Pressure

3-1. Crystal Structures

The crystal structures of the four complexes are solved in the monoclinic $P2_1/n$ space group (No. 14) with $Z = 4$ (Figure 4-1). The summary of the crystal structural data are listed in Table 3-1.[1]

Table 3-1 Crystallographic data for the complexes of [Mn(hfac)$_2$]·(BNO) and [Mn(hfac)$_2$]· (X-BNO) (X = F, Cl and Br).

	[Mn(hfac)$_2$]·(BNO)	[Mn(hfac)$_2$]·(F-BNO)	[Mn(hfac)$_2$]·(Cl-BNO)	[Mn(hfac)$_2$]·(Br-BNO)
Formula	C$_{24}$H$_{24}$N$_2$O$_6$F$_{12}$Mn	C$_{24}$H$_{23}$N$_2$O$_6$F$_{13}$Mn	C$_{24}$H$_{23}$ClN$_2$O$_6$F$_{12}$Mn	C$_{24}$H$_{23}$BrN$_2$O$_6$F$_{12}$Mn
Formula weight	719.38	737.37	753.83	798.28
Space group	$P2_1/n$	$P2_1/n$	$P2_1/n$	$P2_1/n$
a / Å	9.212(3)	9.351(4)	8.953(4)	9.244(4)
b / Å	16.620(3)	16.626(3)	17.020(4)	17.155(5)
c / Å	20.088(2)	20.167(3)	20.094(5)	20.431(7)
β / deg	98.46(1)	100.01(2)	98.66(2)	99.56(3)
V / Å^3	3042(1)	3087(1)	3027(1)	3195(1)
Z	4	4	4	4
Crystal Dimensions / mm^3	$0.30 \times 0.15 \times 0.95$	$0.10 \times 0.10 \times 0.50$	$0.05 \times 0.10 \times 0.10$	$0.20 \times 0.20 \times 0.40$
Diffractometer	Rigaku AFC5R	Rigaku AFC7R	Rigaku Raxis-IV	Rigaku AFC7R
D_{calc} /g cm^{-3}	1.571	1.586	1.654	1.662
Hydrogen	Refined	Fixed calc.	Fixed calc.	Fixed calc.
Observations	3256	3420	2844	1771
Variables	432	415	415	415
R	0.055	0.069	0.106	0.064
R_W	0.058	0.064	0.122	0.026
GOF	1.90	2.96	2.95	2.51
Temperature	Room Temperature	Room Temperature	130 K	Room Temperature

The analyses reveal that the manganese(II) ions have octahedral coordination with four oxygen atoms of two hfac anions and two oxygen atoms of two different BNO's molecules. The molecules of BNO's which are related by a two-fold screw symmetry coordinate to the Mn(II) ion in *cis* configuration. The Mn(II) ion and biradical molecules form a helical one-dimensional polymeric chain structure along the *b*-axis with the alternating manner. The details of the octahedral coordination are listed in Table 3-2. The bond lengths and angles around the Mn atom are listed. The octahedral coordination in four complexes are similar one another. The details of the connection of the atoms on the chain are listed in Table 3-3 and 3-4. The chain structure is similar. The distance between Mn atoms in the chains of the complexes are similar; 9.21, 9.35, 8.95 and 9.24 Å for [Mn(hfac)$_2$]·(BNO) and [Mn(hfac)$_2$]·(X-BNO) (X = F, Cl and Br), respectively. But the angles of [Mn(hfac)$_2$]·(BNO) and [Mn(hfac)$_2$]·(F-BNO) are wider than those of [Mn(hfac)$_2$]·(Cl-BNO) and [Mn(hfac)$_2$]·(Br-BNO). Therefore, the zigzag forms of the chains include small deference.

Table 3-2 Bond lengths between the manganese ion and coordinated oxygen atoms.
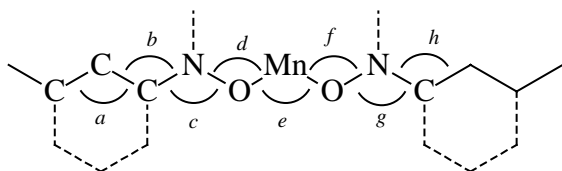
	Bond length					
	Mn – O_1	Mn – O_2	Mn – O_3	Mn – O_4	Mn – O_5	Mn – O_6
X = H	2.10 Å	2.08 Å	2.14 Å	2.14 Å	2.16 Å	2.14 Å
X = F	2.10 Å	2.10 Å	2.15 Å	2.13 Å	2.17 Å	2.15 Å
X = Cl	2.13 Å	2.08 Å	2.14 Å	2.13 Å	2.21 Å	2.15 Å
X = Br	2.14 Å	2.08 Å	2.12 Å	2.12 Å	2.19 Å	2.14 Å

	Angles							
X	O_1-Mn-O_2	O_2-Mn-O_5	O_5-Mn-O_4	O_4-Mn-O_1	O_1-Mn-O_3	O_3-Mn-O_6	O_1-Mn-O_6	O_2-Mn-O_3
H	86.8 °	96.3 °	86.7 °	90.2 °	96.5 °	165 °	96.7 °	96.0 °
F	86.9 °	96.1 °	86.8 °	89.6 °	96.6 °	167 °	95.3 °	94.3 °
Cl	84.6 °	100 °	88.5 °	88.5 °	104 °	167 °	89.8 °	86.1 °
Br	85.0 °	100 °	88.9 °	88.3 °	104 °	166 °	90.4 °	85.9 °
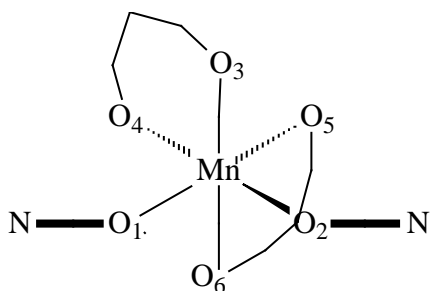
Table 3-3 Bond lengths in the chain structure of the complexes.
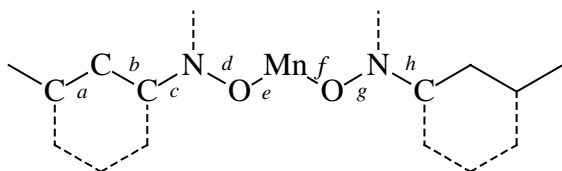
	Bond Position							
	a	*b*	*c*	*d*	*e*	*f*	*g*	*h*
X = H	1.38 Å	1.39 Å	1.42 Å	1.30 Å	2.10 Å	2.08 Å	1.30 Å	1.43 Å
X = F	1.38 Å	1.38 Å	1.44 Å	1.27 Å	2.10 Å	2.10 Å	1.29 Å	1.41 Å
X = Cl	1.37 Å	1.40 Å	1.41 Å	1.32 Å	2.13 Å	2.08 Å	1.31 Å	1.44 Å
X = Br	1.38 Å	1.40 Å	1.42 Å	1.30 Å	2.14 Å	2.08 Å	1.29 Å	1.43 Å

**Table 3-4** Bond angles in the chain structure of the complexes.

|	Angle Position							
	a	*b*	*c*	*d*	*e*	*f*	*g*	*h*
X = H	120 °	122 °	116 °	126 °	86.8 °	124 °	116 °	117 °
X = F	119 °	124 °	116 °	126 °	86.9 °	122 °	117 °	117 °
X = Cl	120 °	122 °	116 °	128 °	84.6 °	123 °	116 °	116 °
X = Br	120 °	123 °	116 °	129 °	85.0 °	125 °	115 °	118 °

The nearest neighboring chain is related by the a-translation symmetry. The short interchain contacts along the *a*-axes are seen between the F atom of hfac molecule and the O atom of the BNO/X-BNO molecule; the F···O distances in the crystal of [Mn(hfac)$_2$]·(BNO) and [Mn(hfac)$_2$]·(X-BNO) (X = F, Cl and Br) are 3.04, 3.16, 3.71 and 3.94 Å, respectively. The three complexes, [Mn(hfac)$_2$]·(X-BNO) (X = F, Cl and Br), have considerably short contact between the F atom of hfac and the halogen atom of X-BNO molecule. X···F distances are 3.16 (X = F), 3.27 (X = Cl) and 3.40 Å (X = Br), respectively. These distances are closely in agreement with the sum of the van der Waals radii (2.94, 3.22 and 3.32 Å, respectively).[2]

In the case of the chain alignment along the *c*-axes, the difference of the chain alignment between the complexes of [Mn(hfac)$_2$]·(BNO), and [Mn(hfac)$_2$]·(F-BNO), and the ones of [Mn(hfac)$_2$]·(Cl-BNO) and [Mn(hfac)$_2$]·(Br-BNO) are larger the one along *a*-axes (Figure 3-2). Since the distances between chains are longer than the one along *a*-axes, it appears that the interactions along c-axes are smaller.
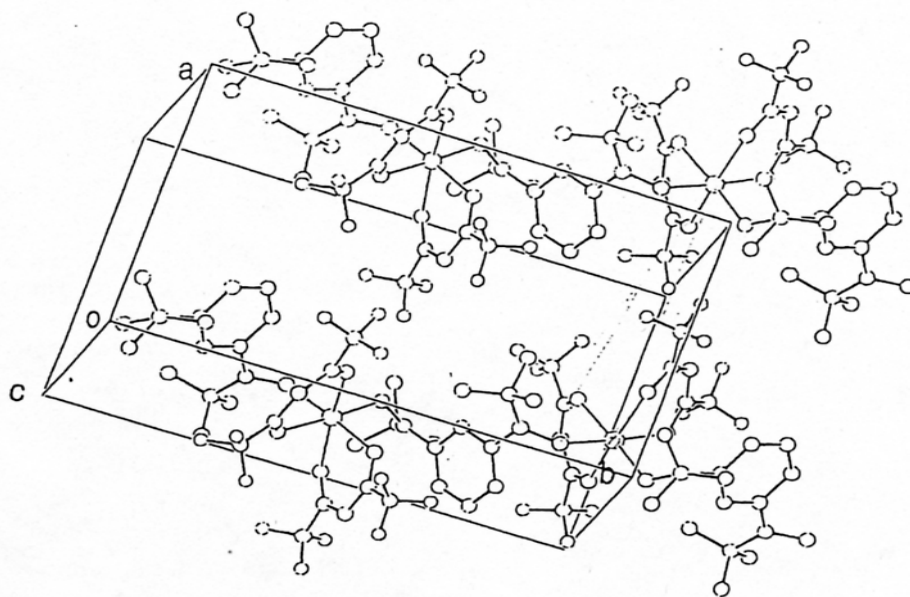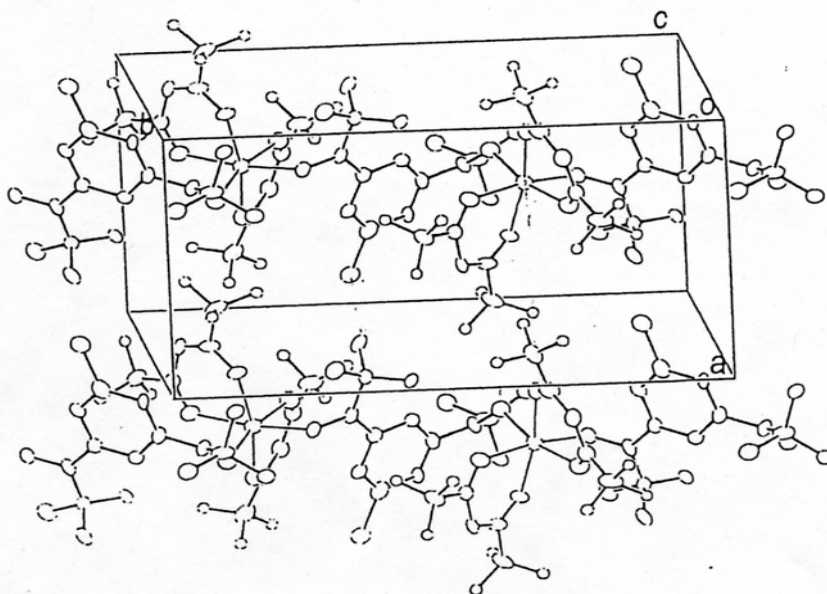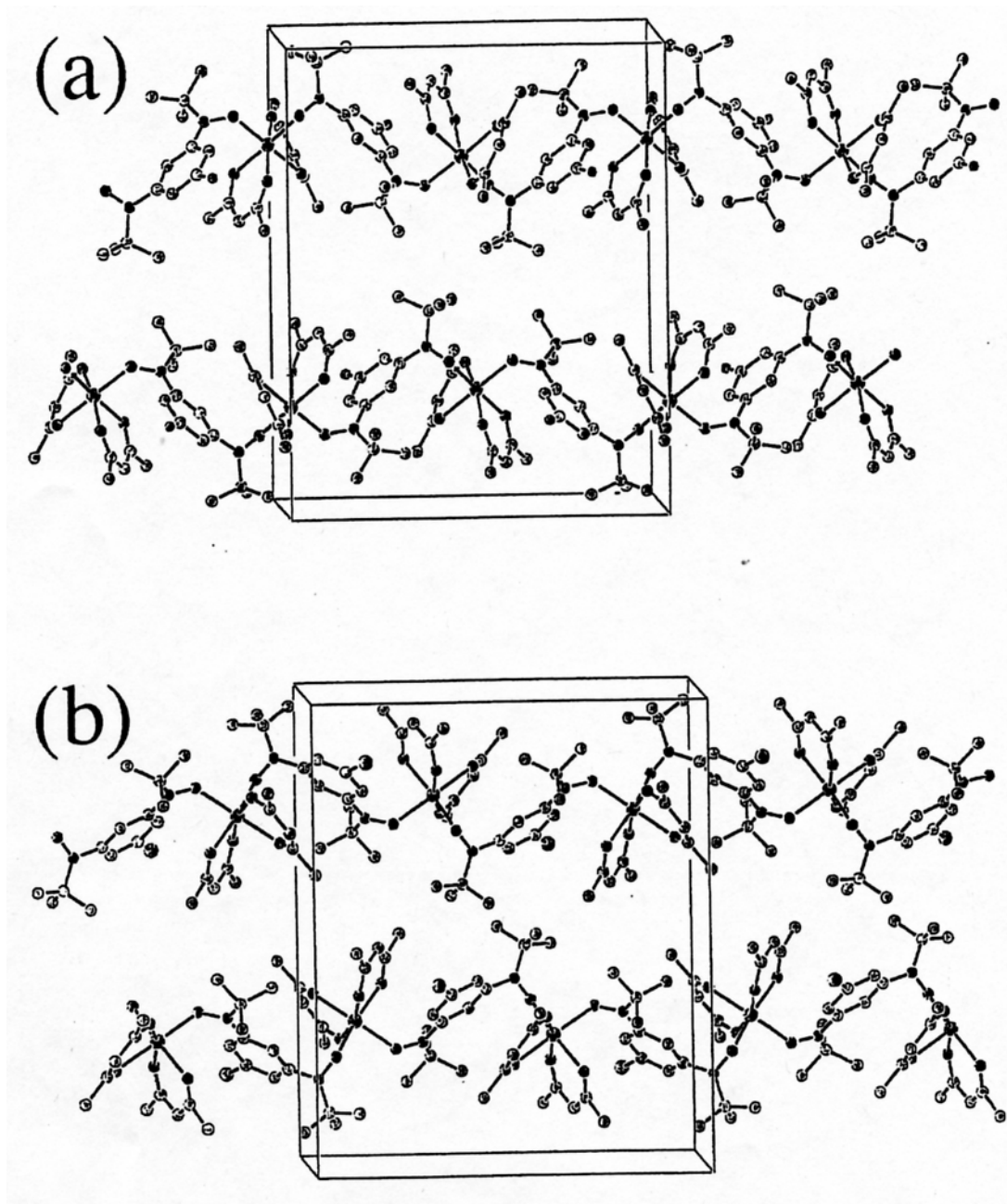
Figure 3-1 The nearest neighboring chains related by the *a*-translation symmetry. (a) [Mn(hfac)$_2$]·(BNO) and (b) [Mn(hfac)$_2$]·(Cl-BNO).

Figure 3-2 The neighboring chains related by inversion chain projected on to the *bc*-plane. (a) [Mn(hfac)₂]·(BNO) and (b) [Mn(hfac)₂]·(Br-BNO)

3-2. Magnetic properties at ambient pressure[1)]

The magnetic structure of the one-dimensional chains of all the complexes are ferrimagnetic due to the strong antiferromagnetic interaction between the two kind of spins of Mn(II) ($S = 5/2$) atom and the NO· radical ($S = 1$) through the coordination bond (Scheme 3-2-1). At the low temperature region, all complexes exhibit the quasi-one-dimensional magnetism due to the weak interchain interaction.
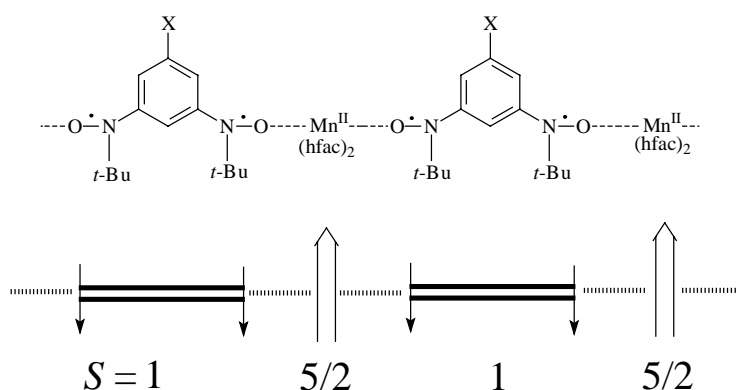

Scheme 3-2-1

[Mn(hfac)$_2$]·(BNO) and [Mn(hfac)$_2$]·(F-BNO) have antiferromagnetic ground states due to an antiferromagnetic interchain interaction below the transition temperatures, T_N = 5.5 and 5.3 K, respectively. The magnetization isotherms below T_N show a spin flip transition at the critical field, H_C, so that they are metamagnets.

[Mn(hfac)$_2$]·(Cl-BNO) and [Mn(hfac)$_2$]·(Br-BNO) have ferrimagnetic ground state due to a ferromagnetic interchain interaction below the transition temperatures, T_C = 4.8 and 5.3 K, respectively. Below T_C, their magnetic behaviors are similar to each other. The magnetization at 1.8 K shows saturation above about 3 T at the value of *ca.* 3.0 μ_B/mol. The complexes show narrow hysteresis with the coercive force less than 20 Oe.

3-2-1. Magnetic Properties of [Mn(hfac)$_2$]·(BNO)

The temperature dependence of the dc susceptibilities (χ_{dc}) at ambient pressure, measured with an applied field of 5 Oe, is shown in Figure 3-2-1. The measurements after zero-field cooling (ZFC) show an abrupt increase of the susceptibility below 7 K, making a sharp peak at 5.4 K. The measurements after field cooling (FC) show the behavior from the hysteresis.
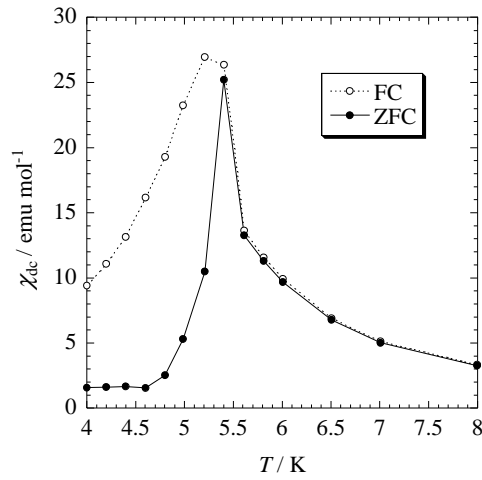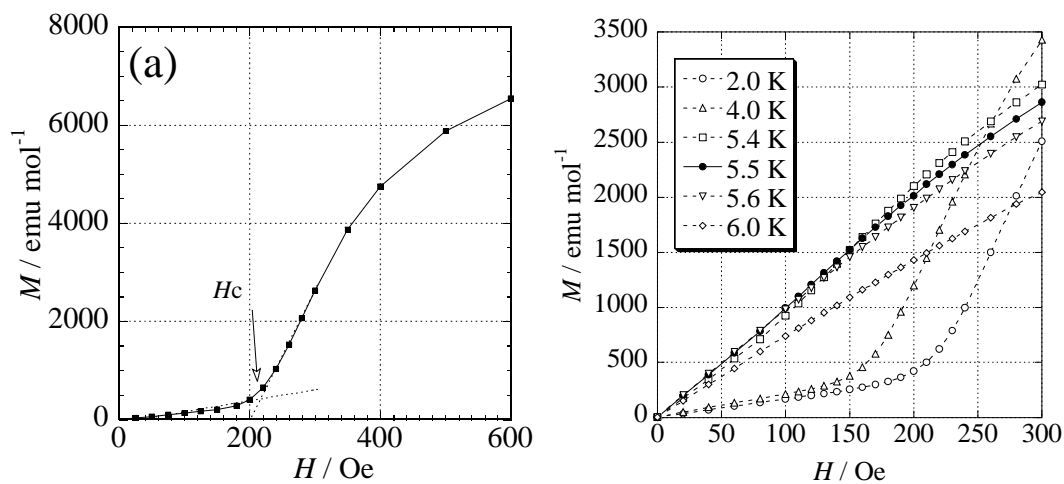

Figure 3-2-1 The temperature dependence of the dc susceptibility of [Mn(hfac)$_2$]·(BNO) at ambient pressure.

The ac susceptibilities also show sharp peaks in both the real part (χ') and the imaginary part (χ'') at the same temperature (Figure 3-2-2). We use the ac measurements to determine T_N under pressure.
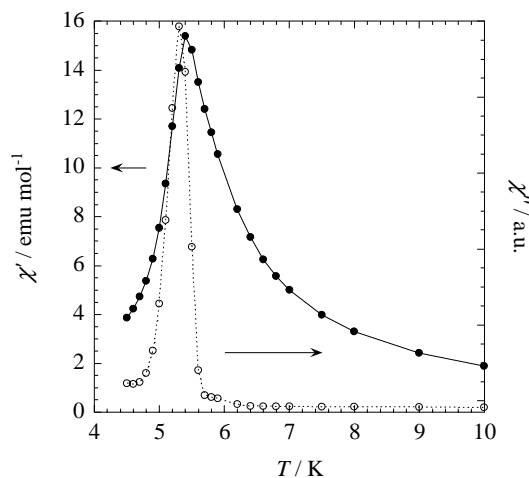
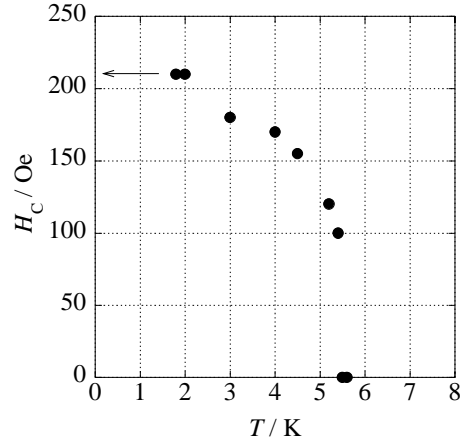**Figure 3-2-2** The temperature dependence of the ac susceptibility $\chi_{ac}(\chi'; \bullet$ and $\chi''; \bigcirc)$ of [Mn(hfac)$_2$]·(BNO) at ambient pressure.

Figure 3-2-3 The field dependence of the magnetization curve at (a) 1.8 K, and 2.0 ~ 6.0 K.

The field dependence of the magnetization curve at several temperatures is shown in Figure 3-2-3. The magnetization curve at 1.8 K shows the weak field dependence below 210 Oe, followed a rapid increase above it. This is spin flip behavior that is characteristic of the metamagnet. With increasing temperature, H_C was

shifted to lower field, and spin flip behavior was disappeared below 5.5 K. Therefore, the temperature at which χ' makes a peak is estimated to T_N.
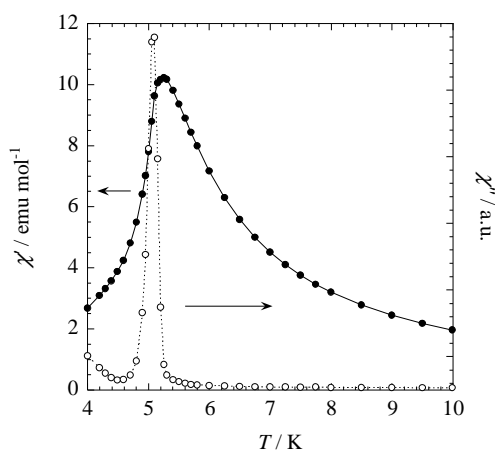

Figure 3-2-4 Temperature dependence of H_C of the spin flip behavior.

Temperature dependence of H_C is shown in Figure 3-2-4. H_C shows a rapid increase with decreasing temperature at around T_N, and almost saturates at around 1.8 K. Therefore, it appears that H_C at absolute zero is almost similar to the one at around 1.8 K.
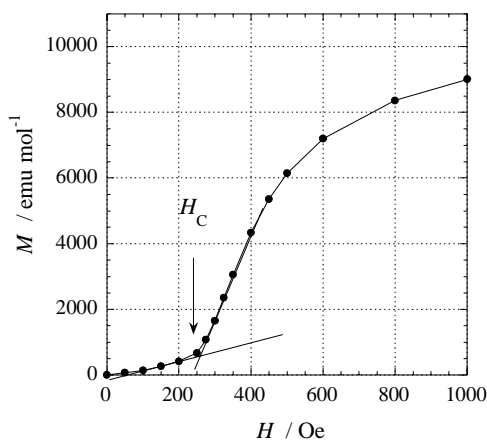
3-2-2. Magnetic Properties of [Mn(hfac)$_2$]·(F-BNO)

The temperature dependence of the ac susceptibility of [Mn(hfac)$_2$]·(F-BNO) is shown in Figure 3-2-5. The χ' value increases with decreasing temperature, and makes the maximum at $T_N = 5.3$ K. Simultaneously, χ'' makes a sharp peak.

Figure 3-2-5 The temperature dependence of the ac susceptibility $\chi_{ac}(\chi'; \bullet$ and $\chi''; \bigcirc)$ of [Mn(hfac)$_2$]·(F-BNO) at ambient pressure.

The magnetization curve of [Mn(hfac)$_2$]·(F-BNO) is shown in Figure 3-2-6. The magnetization curve at 2.0 K is also shown metamagnetic behavior ($H_C \sim 240$ Oe), as well as the case of [Mn(hfac)$_2$]·(BNO).

Figure 3-2-6 Field dependence of the magnetization of [Mn(hfac)$_2$]·(F-BNO) at 2.0 K.

3-2-3. Magnetic Properties of [Mn(hfac)$_2$]·(Cl-BNO)

Figure 3-2-7 shows the temperature dependence of ac susceptibility (χ_{ac}). The real part of the χ_{ac} (χ') showed an abrupt increase at around T_C = 4.8 K with increasing temperature, and reached a maximum at around T_C. The imaginary part of the χ_{ac} (χ'') appeared below T_C, and increased with decreasing temperature.

Below T_C, the magnetization isotherms showed the rapid increases, and approached to the theoretical saturation value ($M_{sat} \sim 16800$ emu/mol) (Figure 3-2-8).

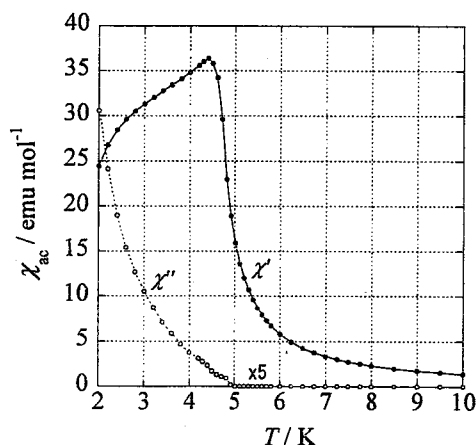**Figure 3-2-7** Temperature dependence of the ac susceptibility (χ' and χ'') of the sample in a capsule.
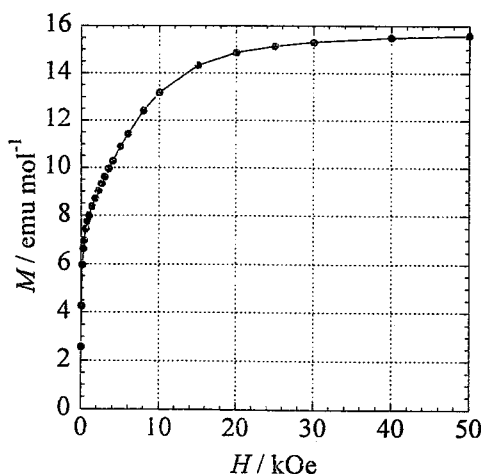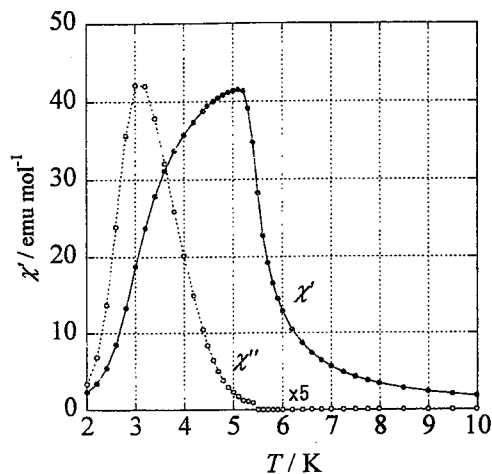

Figure 3-2-8 Field dependence of the magnetization at 2.0 K of the sample in a capsule.

3-2-4. Magnetic Properties of [Mn(hfac)₂]·(Br-BNO)

The temperature dependence of the ac susceptibility of [Mn(hfac)$_2$]·(Br-BNO) at ambient pressure is shown in Figure 3-2-9. The value of χ' show a peak at T_C = 5.3 K. χ'' appears below this temperature, and is increased with decreasing temperature.

Figure 3-2-9 Temperature dependence of the ac susceptibility (χ' and χ'') of the sample in a capsule (χ';●, χ'';○).

The magnetization isotherms at 1.8 K shows a rapid increase, and approached to the theoretical saturation value (M_{sat} ~ 16800 emu/mol) (Figure 3-2-10).
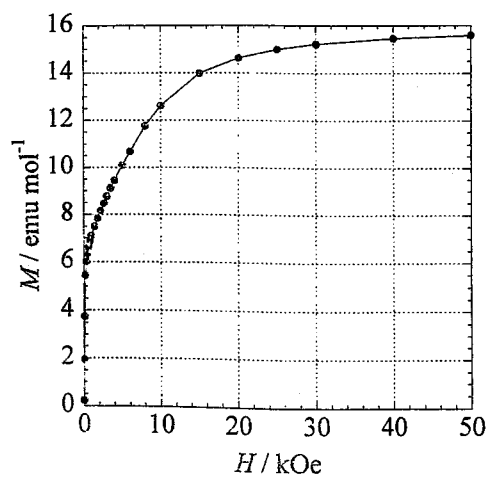
**Figure 3-2-10** Magnetization curve of [Mn(hfac)$_2$]·(Br-BNO) at 1.8 K.

References

1) H. Iwamura and K. Inoue, in *Magnetism: Molecules to Materials II* Ed. by J. S. Miller and M. D. Drillon, Wiley-VCH, Weinheim (**2001**) p. 61.

2) A Bobdi, *J. Phys. Chem.*, 68 (**1964**) 441-445.

3) A. S. Markosyan, H. Iwamura and K. Inoue, *Mol. Cryst. Liq. Cryst.*, 334 (**1999**) 549-568.

4. Pressure Effect in Metamagnets, [Mn(hfac)$_2$] $\cdot$ (BNO) and [Mn(hfac)$_2$]$\cdot$(F-BNO)

Y. Hosokoshi, K. Suzuki, K. Inoue and H. Iwamura," Pressure Effect on Mn Complexes of Bisaminoxyl Radicals", *Mol. Cryst. Liquid. Cryst.,*334 (**1999**) 511

4-1. Pressure Effect in a Metamagnet, [Mn(hfac)$_2$]·(BNO)

The magnetic behavior of the complex of [Mn(hfac)$_2$]·(BNO) in the hydrostatic pressure up to 11 kbar was studied. Figure 4-1-1 shows the temperature dependence of the ac susceptibility (χ_{ac}) at ambient pressure ($p = 0$) and under high pressures ($p < 11$ kbar). At $p = 0$, the transition temperature (T_N) was 5.5 K. With increasing pressure, T_N at which χ' made the peak shifted to higher temperature. The peak of the imaginary part of χ_{ac} (χ'') near T_N also shifted to higher temperature with increasing pressure.
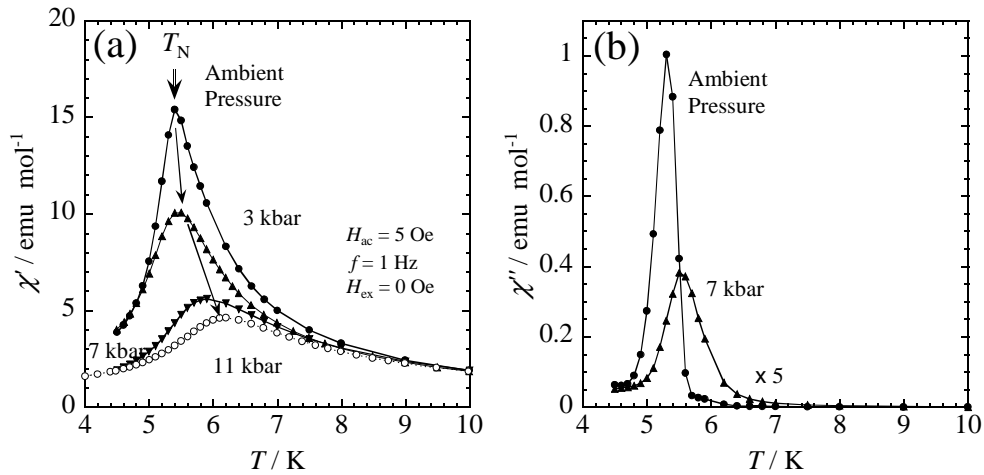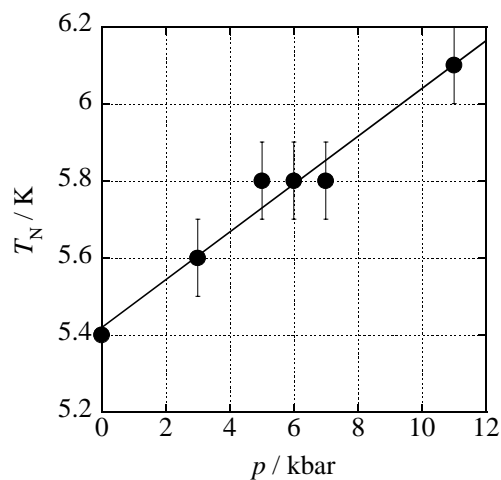

Figure 4-1-1 Temperature dependence of ac susceptibility at ambient pressure(●) and under pressure ($p = 3$(▲), 7 kbar(▼) and 11 kbar(○)).(a) the real part of χ_{ac}(χ'), and (b) the imaginary part of χ_{ac}(χ'').
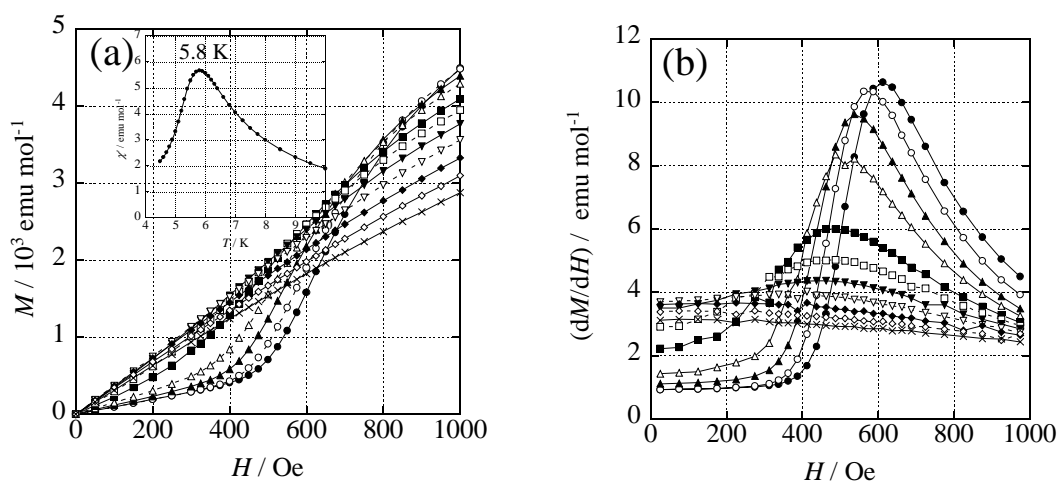
Figure 4-1-2 shows the pressure dependence of $T_N(p)$. This is characterized with the following positive and liner pressure dependence below 11 kbar,

$$T_N(p) = T_N(p_0)(1 + 0.012p), \qquad\qquad [4\text{-}1]$$

where $T_N(p_0)$ is T_N at ambient pressure.

Figure 4-1-2 Pressure dependence of T_N for [Mn(hfac)$_2$]·(BNO)

Figure 4-1-3 (a) The temperature dependence of magnetization isotherms under 6 kbar, and (b) the field derivatives of magnetization s against field. $T = 2.0(\bullet)$, $3.0(\bigcirc)$, $4.0(\blacktriangle)$, $4.5(\triangle)$, $5.0(\blacksquare)$, $5.25(\square)$, $5.5(\blacktriangledown)$, $5.75(\triangledown)$, $6.0(\blacklozenge)$, $6.25(\lozenge)$ and 6.5 K($\times$). Insert: Temperature dependence of χ_{ac} under 6.0 kbar.

The temperature dependence of the magnetization curves under 6 kbar is shown in Figure 4-1-3. The critical field of the spin flip behavior (H_C) at 2.0 K under 6

kbar was estimated to be *ca.* 500 Oe, and H_C was shifted to lower field with increasing temperature. The plots of the field derivatives of the magnetizations against field (dM/dH) indicate the spin flip field as a peak. The peak disappears above 6.0 K. This temperature agrees with T_N at which χ' makes the peak.
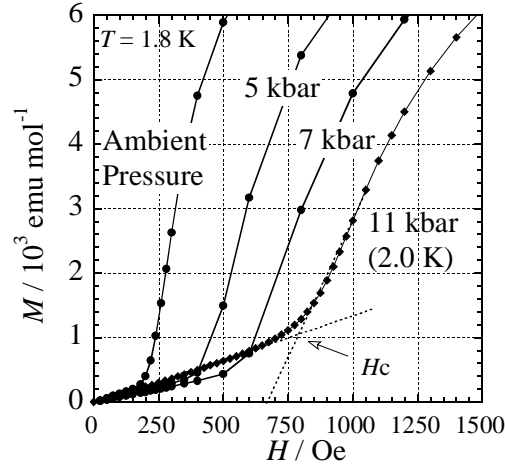

Figure 4-1-4 Temperature dependence of the magnetization curves at ambient pressure and under 5 and 7 kbar (1.8 K), and 11 kbar (2.0 K).

The pressure dependence of the magnetization curves is shown in Figure 4-1-4. The H_C values shifted to higher field with increasing pressure. Figure 4-1-5 shows the pressure dependence of $H_C(p)$. The H_C values are monotonously increased with pressure, and the relationship is characterized with the following positive and linear pressure dependence below 11 kbar.

$$H_C(p) = H_C(p_0)(1 + 0.25p), \qquad\qquad [4\text{-}2]$$

where $H_C(p_0)$ is H_C at ambient pressure.
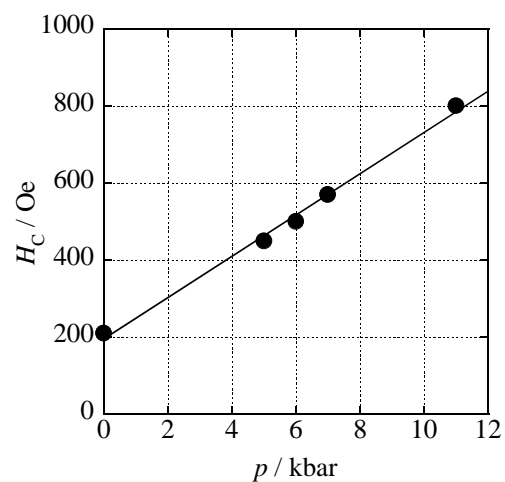
Figure 4-1-5 Pressure dependence of the HC for [Mn(hfac)$_2$]·(BNO).

In the case of [Mn(hfac)$_2$]·(BNO), H_C and T_N are monotonously enhanced by pressure. T_N and H_C value are related to the interchain interaction. This result suggests the simple enhancement of interchain interaction. It appears that this enhancement comes from a reduction of the interchain distances by pressurization.

4-2. Pressure Effect in Metamagnet, [Mn(hfac)$_2$]·(F-BNO)

The magnetic behavior of the complex of [Mn(hfac)$_2$]·(F-BNO) in the hydrostatic pressure up to 6 kbar was studied.

The temperature dependence of χ_{ac} was shown in Figure 4-2-1. At $p = 0$, χ' was shown the peak at $T_N = 5.3$ K. With increasing pressure, the T_N at which χ' made the peak shifted to higher temperature. The peak of χ'' near T_N also shifted to higher temperature with increasing pressure.
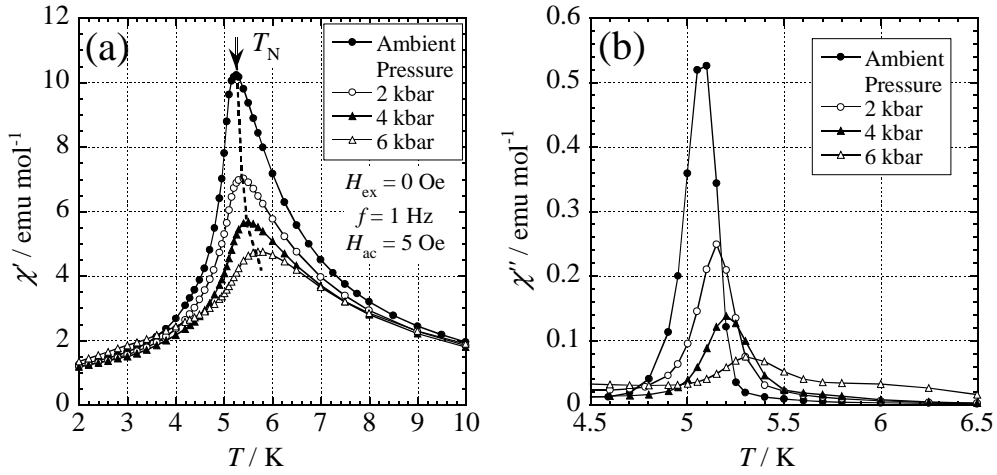
Figure 4-2-1 Temperature dependence of ac susceptibility (χ_{ac}) under several pressures. (a) The real part of $\chi_{ac}(\chi')$ and (b) the imaginary part of $\chi_{ac}(\chi'')$

Figure 4-2-2 shows the pressure dependence of $T_N(p)$. This is characterized with the following positive pressure dependence below 6 kbar,

$$T_N(p) = T_N(p_0)(1 + 0.014p),$$ [4-3]
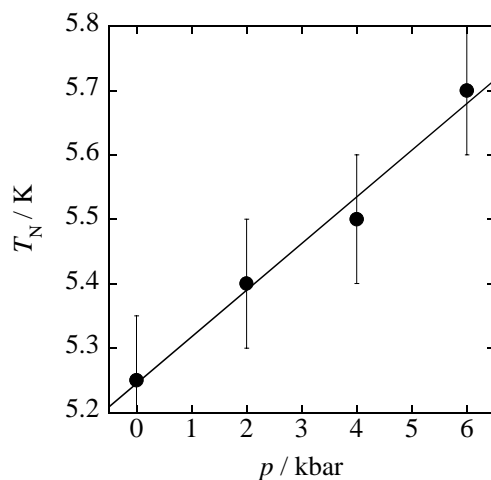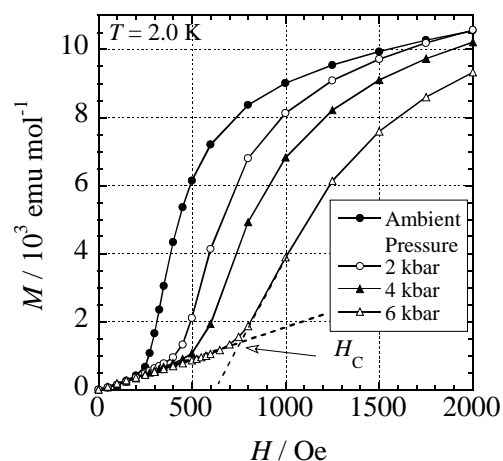
where $T_N(p_0)$ is T_N at ambient pressure.

Figure 4-2-2 The pressure dependence of T_N for [Mn(hfac)$_2$]·(F-BNO)

Figure 4-2-3 The pressure dependence of the magnetization curves under several pressures at 2.0 K.

Figure 4-2-3 shows the pressure dependence of the magnetization curves at 2.0 K. The H_C values shifted to higher field with increasing pressure. Figure 4-2-4 shows the pressure dependence of $H_C(p)$. The H_C values are monotonously increased with pressure, and relationship characterized with the following positive pressure dependence below 6 kbar.

$$H_C(p) = H_C(p_0)(1 + 0.28p), \qquad [4-4]$$

where $H_C(p_0)$ is T_N at ambient pressure ($H_C(p_0) = 280$ Oe).
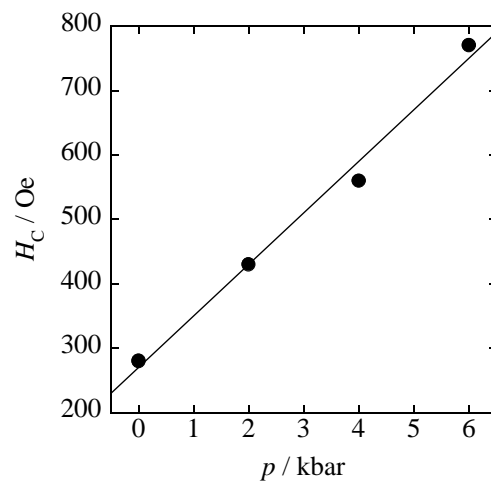
Figure 4-2-4 The pressure dependence of H_C for [Mn(hfac)$_2$]·(F-BNO).

In the case of [Mn(hfac)$_2$]·(F-BNO), TN and HC are also monotonously enhanced by pressure, as well as the case of [Mn(hfac)$_2$]·(BNO). It appears that the pressure dependence of magnetic behavior is similar to the case of [Mn(hfac)$_2$]·(BNO).
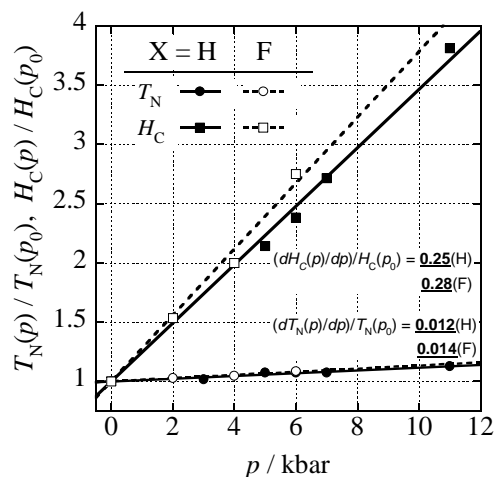
4-3. Conclusion

Figure 4-3-1 **Pressure dependence of T_N and H_C of [Mn(hfac)$_2$]·(BNO) and [Mn(hfac)$_2$]·(F-BNO). The value is optimized by the values at ambient pressure.**

The applied pressure simply enhanced of the magnetic parameters, T_N and H_C in [Mn(hfac)$_2$]·(BNO) and [Mn(hfac)$_2$]·(F-BNO). Figure 4-3-1 shows the pressure dependence of T_N and H_C of the two complexes. The two complexes exhibit similar dependence in T_N and H_C; the slope of T_N (d$T_N(p)$/dp) are 0.012 and 0.014 / kbar, and those of H_C (d$H_C(p)$/dp) are 0.25 and 0.26 / kbar, for [Mn(hfac)$_2$]·(BNO) and [Mn(hfac)$_2$]·(F-BNO), respectively.

The reason of the enhancements of T_N and H_C are probably a reduction of the interchain distances by the pressure. The several experimental results of the pressure effects on molecule-based metamagnets and antiferromagnets are listed in Table 4-1. This pressure response is a major case for a molecule-based magnetic material with antiferromagnetic interaction. Many antiferromagnets and metamagnets show positive enhancement of T_N. Pressure dependences of [Mn(hfac)$_2$]·(BNO) and [Mn(hfac)$_2$]·(F-BNO) are identified with the major group.

Table 4-1 Pressure dependence of T_N and H_C of molecule-based anti- / metamagnets.

Compound	T_N / K	a / kbar*	H_C / kOe	a' / kbar*	Ref.
(metamagnet)					
[Mn(hfac)$_2$]·(BNO)	5.5	0.012	0.21	0.25	
[Mn(hfac)$_2$]·(F-BNO)	5.3	0.014	0.28	0.28	
FeBr$_2$	14.1	0.058	28.8	0.059	1
FeCl$_2$ ($p \leq 1.85$ kbar)	22.9	0.011	10.45	0.070	2
FeCl$_2$ ($p > 1.85$ kbar)	24.8	0.027	10.68	0.073	2
(antiferromagnet)					
MnBr$_2$·4H$_2$O	2.12	0.014	—	—	3
Mn(HCOO)$_2$·2H$_2$O	3.68	0.011	—	—	4
CoCl$_2$·6H$_2$O	2.29	0.028	—	—	5
CuCl$_2$·2H$_2$O	4.36	0.022	—	—	6
DMMC	3.60	0.038	—	—	7
TMMC ($p > 3.2$ kbar)	0.84	0.049	—	—	7
TMMC ($p < 3.2$ kbar)	0.84	0.026	—	—	7
p-Cl-BDPA	3.25	0.019	—	—	8
TANOL	0.49	0.058	—	—	9
TPV (weak FM)	1.78	0.093	—	—	10
TOV (weak FM)	5.5	0.086	—	—	11

*) $a = (\mathrm{d}T_N(p)/\mathrm{d}p)/\mathrm{d}T_N(p_0)$, $a' = (\mathrm{d}H_C(p)/\mathrm{d}p)/\mathrm{d}H_C(p_0)$.

References

1) C. Vettier, H. L. Alberts and D. Bloch, *Phys. Rev. lett.*, *31* (**1973**) 1414.

2) (a) C. Vettier and E. B. Yellon, *Phys. Rev., B11* (**1975**) 4700, (b) A. Liowsski and Z. Oryszkiewicz, *Phys. Stat. Sol. (b) 131* (**1985**) K117.

3) W. A. Ortiz and F. P. Missel, *Phys. Rev., B24* (**1981**) 4013.

4) K. Takeda, K. Koyama and K. Yamagata, *J. Phys. Soc. Jpn., 55* (**1986**) 3725.

5) M. Wada, K. Takeda, A. Ohtani, A. Onodera and T. Haseda, *J. Phys. Soc. Jpn., 52* (**1983**) 3188.

6) K. Takeda, T. Idogaki, K. Tsuru, N. Uryu and M. Inoue, *Jpn. J. Appl. Phys, 26-3* (**1987**) 863.

7) K. Takeda and T. Suzuki, *Jpn. J. Appl. Phys., 26-3* (**1987**) 859.

8) J. Yamaguchi, K. Takeda and M. Inoue, *Chem. Lett.,* (**1990**) 1551.

9) K. Takeda, N. Uryu, M. Inoue and J. Yamaguchi, *J. Phys. Soc. Jpn., 56* (**1987**) 736

10) J. Yamauchi, K. Takeda and K. Konishi, *Mol. Cryst. Liq. Cryst., 233* (**1993**) 97-104.

11) M. Mito, M. Hitaka, T. Kawae, K. Takeda, K. Suzuki and K. Mukai, *Mol. Cryst. Liq. Cryst., 334* (**1999**) 369-378.

# 5. Pressure Effect in a Ferrimagnet, [Mn(hfac)$_2$]·(Br-BNO)

K. Suzuki, Y. Hosokoshi and K. Inoue, "Pressure-induced Metamagnetic Behavior in a Quasi-One-Dimensional Molecule-based Ferrimagnet", *Chem. Lett.*, *3* (**2002**) 316-317

5-1. Magnetic Properties in the Pressure Region of $p = 0 \sim 3.5$ kbar
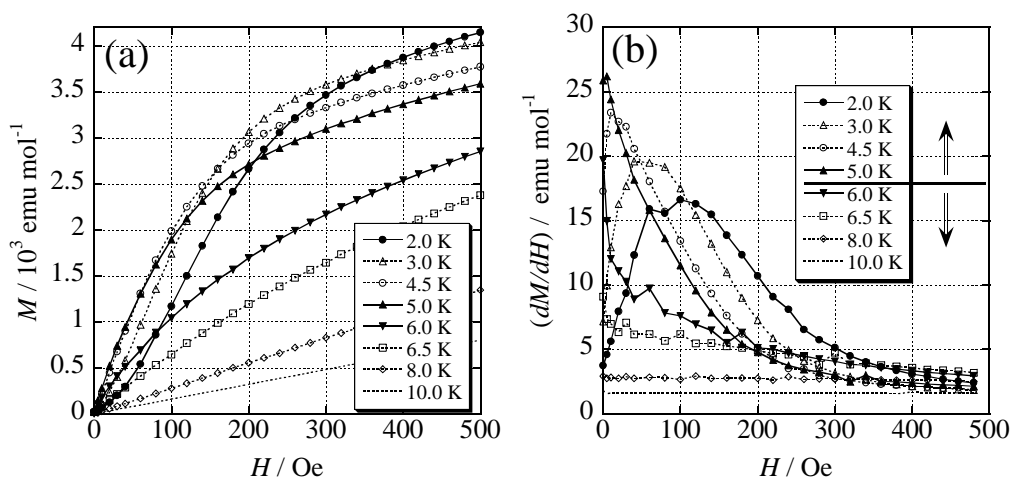
Figure 5-1-1 shows temperature dependence of the ac susceptibility (χ_{ac}) under pressures of $p = 0$, 2, 3 and 3.5 kbar. At $p = 0$, the real part of χ_{ac} (χ') rapid increases below *ca.* 5 K, with a maximum gradient at $T_C = 5.3$ K. The imaginary part of χ_{ac} (χ'') appears below T_C and increases with decreasing temperature. With increasing pressure up to 3.0 kbar, rapid increases of χ' is also shown, and χ'' appeared at 5.3 and 5.4 K under 2.0 and 3.0 kbar, respectively. This behavior is related to the ferrimagnetism. When we applied the pressure larger than $p = 3.5$ kbar, the χ_{ac} behavior was changed. The remarkable difference behavior is the maximums in χ' and χ''. They showed the peaks at *ca.* 5.5 K.
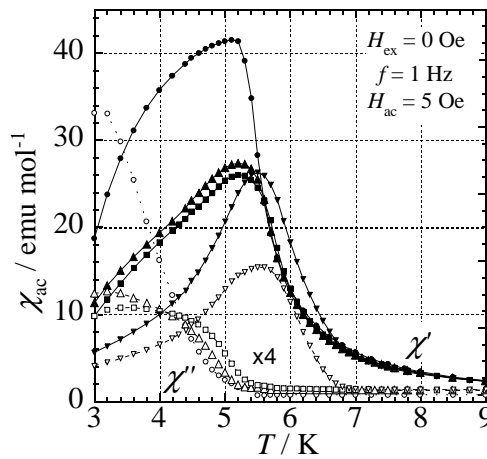
Figure 5-1-1 The temperature dependence of the ac susceptibility at ambient pressure(χ'; ●, χ''; ○) and under $p = 2.0$(χ'; ▲, χ''; △), 3.0(χ'; ■,χ''; □) and 3.5 kbar(χ';▼, χ''; ▽).
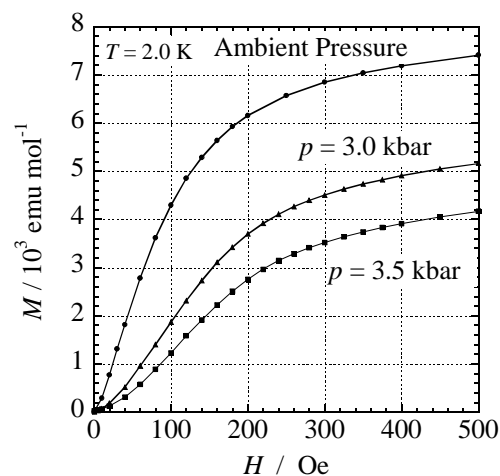
Figure 5-1-2 The pressure dependence of magnetization isotherms at ambient pressure and under p = 3.0 and 3.5 kbar.

Figure 5-1-3 (a) The temperature dependence of magnetization curves under p = 3.5 kbar, and (b) the dM/dH against field

Figure 5-1-2 shows the field dependence of magnetization at 2.0 K under several pressures of p = 0, 3.0 and 3.5 kbar. At p = 0 and 3.0 kbar, the magnetization curves showed rapid increases below *ca.* 500 Oe, and saturated. At 3.0 kbar, magnetization curve is also shown rapid increases with increasing field, and the saturation rate of magnetization became smaller than the one at p = 0. At 3.5 kbar, the magnetization behavior is changed. At 2.0 K, The bend of the magnetization curve at

ca. 50 Oe is noticeable. Figure 5-1-3 shows the field dependence of magnetization curve at several temperatures. The bends in magnetizations curve are recognized as the maxima in the plot of field derivatives of magnetizations against the field (dM/dH). This bending in magnetization is related to the spin flip behavior in a metamagnet. This spin-flip behavior is noticeable below 5.0 K, at which χ' and χ'' takes a maximum. The observed maximum in χ_{ac} is understood as the metamagnetic phase transition when the magnetization curves are taken into account.
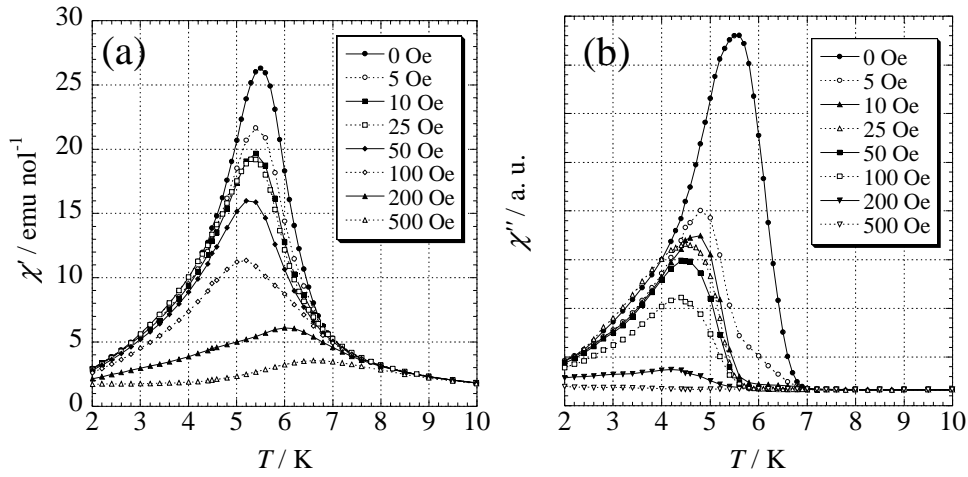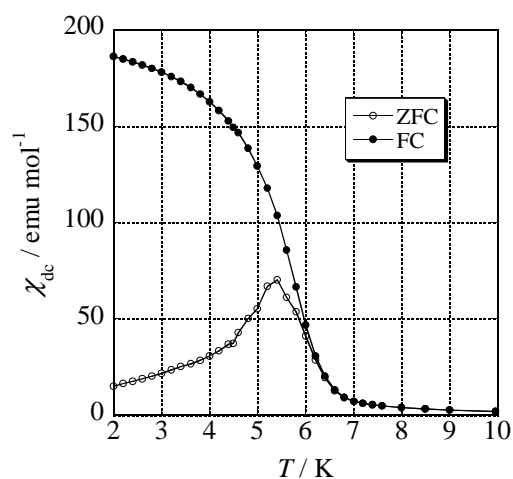

Figure 5-1-4 Temperature dependence of ac susceptibility under $p = 3.5$ kbar with several fields ($H_{ex} = 0 \sim 500$ Oe).

The temperature dependence of χ_{ac} under 3.5 kbar in the field region of $H_{ex} = 0 \sim 500$ Oe is shown in Figure 5-1-4. With increasing field up to 100 Oe, the peak of χ' is shifted to lower temperature. It is characteristic behavior of the metamagnetism. χ'' appeared below 7.0 K and made a peak at 5.5 K under $H_{ex} = 0$ Oe. With increasing field, χ'' behavior changed. Above 25 Oe, χ'' appeared below 5.5 K and made a maximum at 4.5 K. This behavior is suggested the contamination of the ferromagnetic portion with the metamagnetic one. Figure 5-1-5 shows the temperature dependence of χ_{dc}. The value of χ_{dc} in FC measurement is larger than the one in ZFC measurement

below *ca.* 6.5 K. This behavior is related to the mixed ferromagnetic portion. Since the magnetization curve has no anomaly, it appears that the amount is very small.
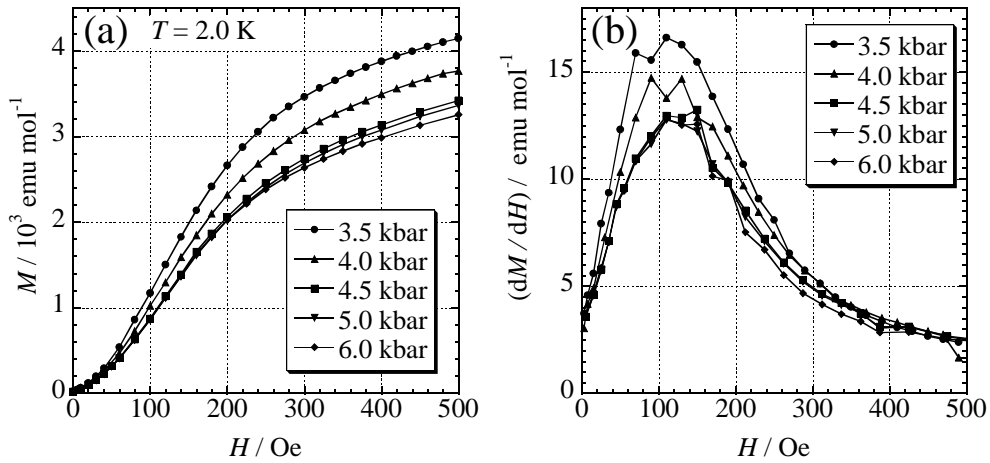

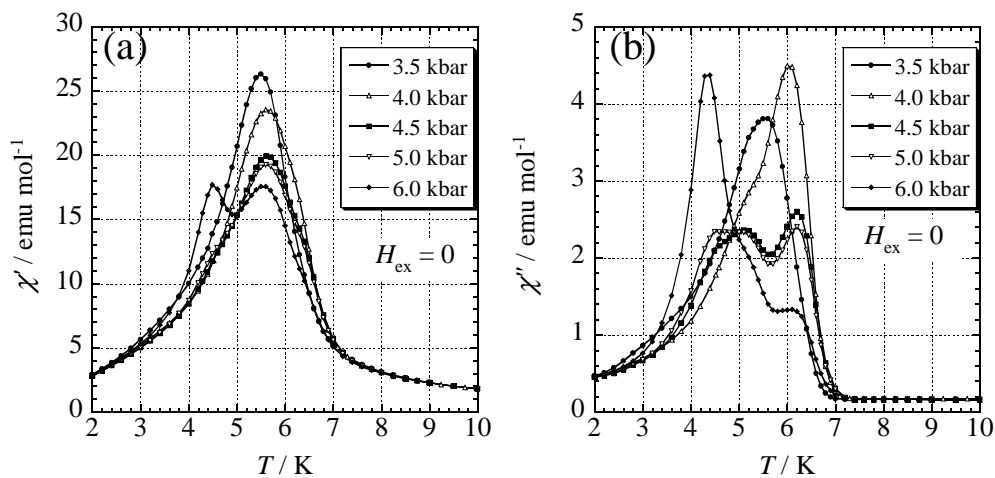**Figure 5-1-5** Temperature dependence of dc susceptibility under p = 3.5 kbar.

In conclusion of this section, we observed the pressure-induced crossover between ferrimagnetic and metamagnetic states at $p \geq 3.5$ kbar. This is the first case of the quasi-one-dimensional molecule-based magnet. However, the ferrimagnetic portions are contaminated.

5-2. Magnetic Properties in the Pressure Region of p = 3.5 ~ 6.0 kbar

Field dependence of the magnetization at 2.0 K in the pressure region of p = 3.5 ~ 6.0 kbar is shown in Figure 5-2-1(a). The spin flip behavior was shown in all pressure regions. The magnetic behaviors in this pressure region are related to the metamagnetism. The plots of the field derivatives of the magnetizations against field (dM/dH) indicate the spin flip field as a peak. With increasing pressure, the peak of dM/dH was shifted to higher field. This result suggests that H_C is shifted to higher field with increasing pressure.
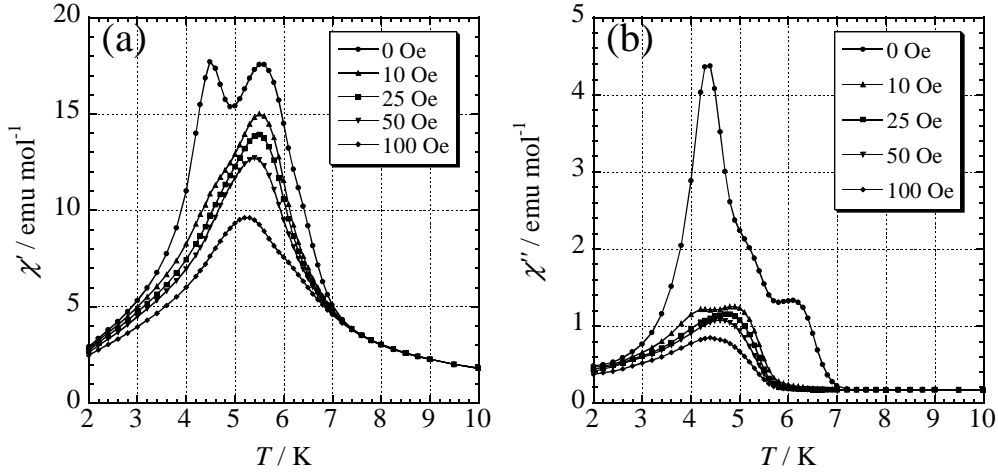

Figure 5-2-1 (a) The pressure dependence of magnetization isotherms under several pressures p = 3.5 ~ 6.0 kbar, and (b) the field derivatives of magnetizations against field.
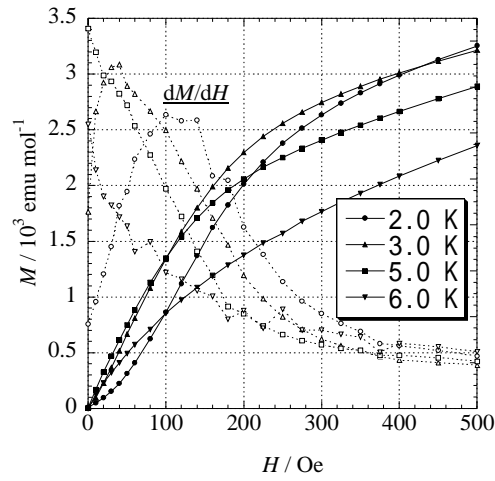
Figure 5-2-2 The temperature dependence of ac susceptibility (χ_{ac}) under $p = 3.5 \sim 6.0$ kbar. (a) The real part of χ_{ac} (χ') and (b) the imaginary part of χ_{ac}(χ'')

Temperature dependence of χ_{ac} in the pressure region of $p = 3.5 \sim 6.0$ kbar is shown in Figure 5-2-2. With increasing pressure, χ_{ac} behaviors became complication. At 3.5 kbar, χ' and χ'' made a peak at 5.5 K. At 4.5 kbar, χ' also made a peak at 5.6 K, and broad shoulder was shown at around 6.5 K. χ'' made a peak at 6.0 K and shoulder was shown at around 5 K. Above 5.0 kbar, a new peaks appeared at 4.5 K in χ' and χ''.
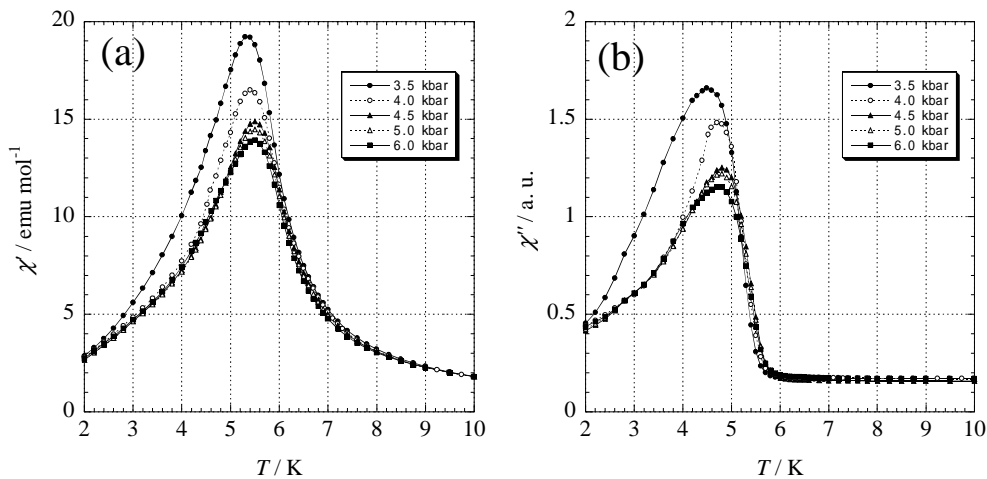
Figure 5-2-3 The temperature dependence of ac susceptibility (χ_{ac}, p = 6.0 kbar) under several external fields H_{ex} = 0 ~ 100 Oe (a) The real part of χ_{ac} (χ') and (b) the imaginary part of χ_{ac}(χ'')

In order to make clear the magnetic behavior in this pressure region, we performed measurements of χ_{ac} under several external static fields (H_{ex}). Figure 5-2-3 shows the temperature dependence of ac susceptibility under 6.0 kbar in the external field region of H_{ex} = 0 ~ 100 Oe. The additional peak at 4.5 and the shoulder at around 6.5 K disappeared above the H_{ex} = 25 Oe, whereas the peak at 5.5 K still remains. It appears that the peak and the shoulder are due to ferromagnetic mixture, as well as the one at 3.5 kbar. The external field of 25 Oe applied, is enough to saturate the ferromagnetic portion. The peak under 25 Oe is related to the transition temperature. The magnetization curve showed the spin flip behavior above 5.0 K, as shown in Figure 5-2-4.

Figure 5-2-4 The temperature dependence of magnetization isotherms under 6 kbar.

The pressure dependences of χ' under external field of $H_{ex} = 25$ Oe, are shown in Figure 5-2-5. When we apply external static fields of $H_{ex} = 25$ Oe, the behavior of χ_{ac} is simplified. T_N at which χ' under 25 Oe made a peak was shifted to higher temperature with increasing pressure. The variation of the pressure dependence of T_N became slowly above $p = 4.5$ kbar. The results mean the enhancement of the interchain antiferromagnetic interaction by applied pressure.

Figure 5-2-5. The temperature dependence of ac susceptibility (χ_{ac}) under 25 Oe in the pressure region of $p = 3.5 \sim 6.0$ kbar. (a) the real part of χ_{ac} (χ') and (b) the imaginary part of χ_{ac} (χ'').

5-3. Magnetic Properties in the Pressure Region of p = 6.0 ~ 10.0 kbar

The field dependence of magnetization curve under several pressures is shown in Figure 5-3-1. The spin-flipping behavior was shown. H_C at which dM/dH made a peak was shifted to lower field with increasing pressure.
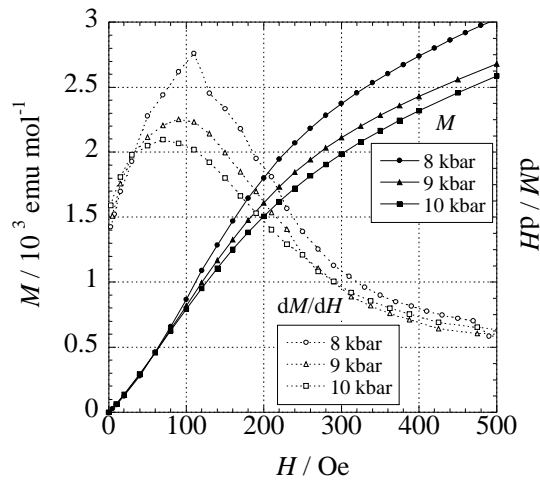

Figure 5-3-1 The field dependence of magnetization curve and the field derivatives of magnetizations against field under p = 8, 9 and 10 kbar.

The temperature dependence of χ_{ac} susceptibility under 8 ~ 10 kbar is shown in Figure 5-3-2. At 8.0 kbar, χ' showed a peak at 4.7 K and the shoulder at around 6 .0 K. With increasing pressure, the shoulder is disappeared and χ' showed only a peak at 4.6 K under 9.0 and 10.0 kbar.
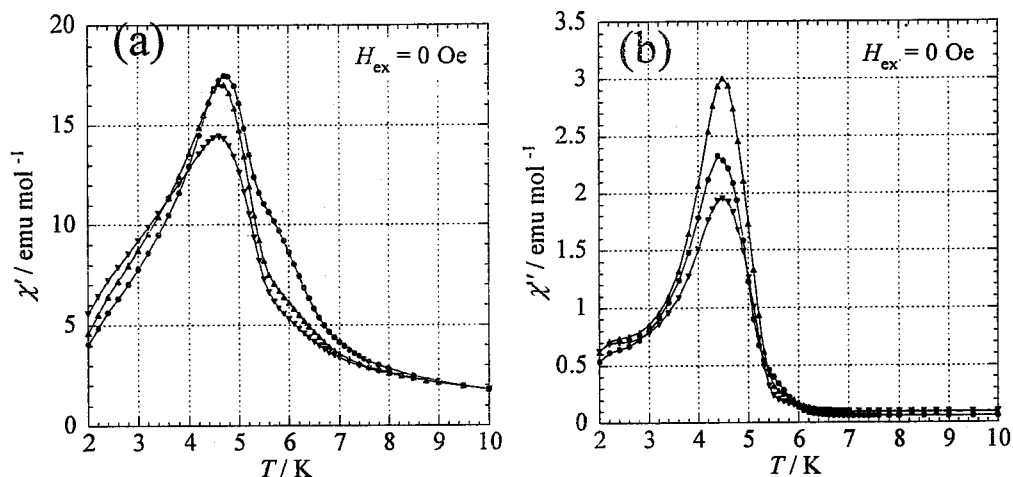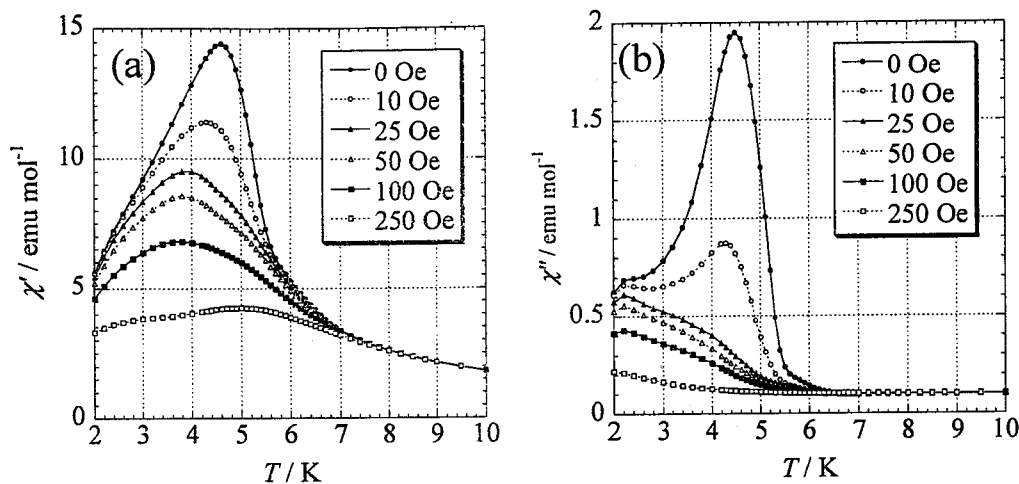
Figure 5-3-2 The temperature dependence of ac susceptibility (χ_{ac}) under H_{ex} = 0 Oe ((a) χ' and (b) χ''), p = 8.0(●), 9.0(▲) and 10 kbar(▼).

The temperature dependence of χ_{ac} under 8.0 kbar in several external fields is shown in Figure 5-3-3. The peak at 4.7 K was decreased with increasing field up to 25 Oe, and a new peak appeared at around 5.1 K. This behavior is similar to the one under 6.0 kbar. Transition temperature is estimated at 5.1 K due to the peak of χ' under 25 Oe.
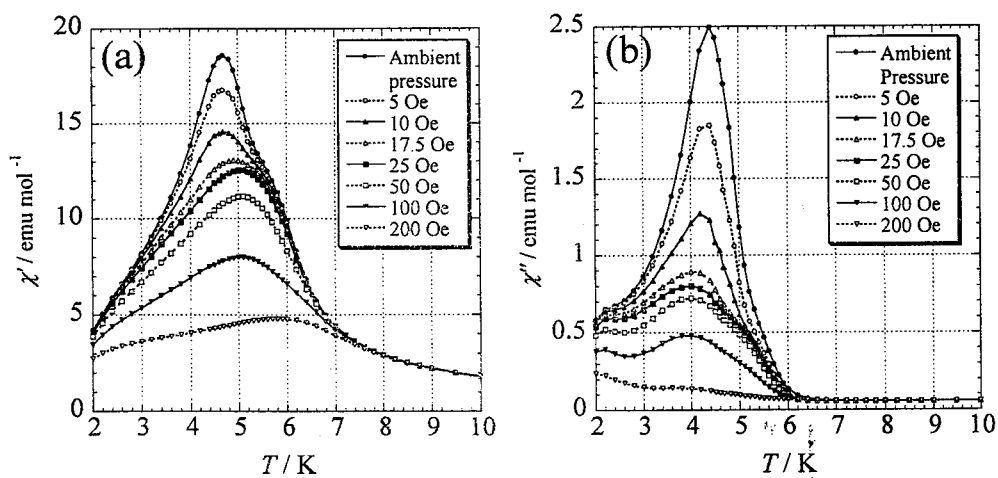
**Figure 5-3-3** The temperature dependence of ac susceptibility (χ_{ac}, p = 8.0 kbar) under several external fields H_{ex} = 0 ~ 200 Oe (a) The real part of χ_{ac} (χ') and (b) the imaginary part of χ_{ac}(χ'').

Figure 5-3-4 The temperature dependence of ac susceptibility (χ_{ac}) under 10 kbar; $H_{ex} = 0 \sim 250$ Oe. (a) The real part of χ_{ac} (χ') and (b) the imaginary part of χ_{ac} (χ'').

The temperature dependence of χ_{ac} under 10 kbar with several external fields is shown in Figure 5-3-4. Under $H_{ex} = 0$, χ' made a peak at 4.6 K. With increasing pressure up to 100 Oe, the peak of χ' was shifted to lower temperature. From this result, T_N is estimated to 4.6 K by the temperature of the peak of χ' under $H_{ex} = 0$. The spin flip behavior in the magnetization curve showed above 4.5 K. This temperature is consistent in T_N.
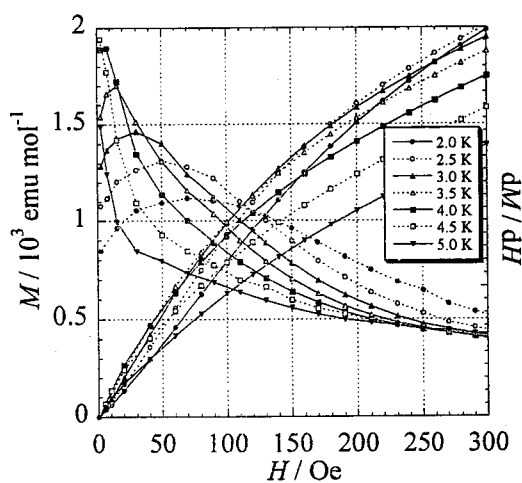
Figure 5-3-5 The field dependence of magnetization curve and the field derivatives of magnetizations against field under $p = 10$ kbar at several temperatures $T = 2.0 \sim 5.0$ K.
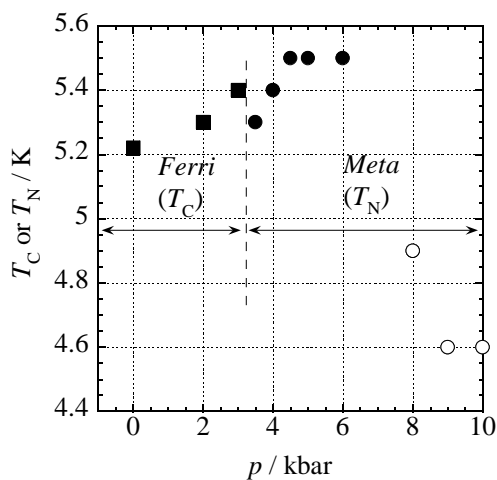
In this pressure region, the metamagnetic behavior is observed. But the pressure dependence of transition temperature is different with the one below 6.0 kbar; T_N is shifted to lower temperature with increasing pressure.

5-4. Conclusion

The pressure dependence of the magnetic properties of $[Mn(hfac)_2] \cdot (Br\text{-}BNO)$ is studied. We observed the pressure-induced crossover between ferrimagnetic and metamagnetic states at $p \geq 3.5$ kbar. It can be said that the interchain ferromagnetic interactions are not stable at high pressure. The interchain ferromagnetic interactions could stand on the strict condition of special molecular overlapping. The pressure induced change from ferromagnetic to antiferromagnetic states, is also reported in genuine organic ferromagnets, β-p-NPNN[1] and p-Cl-Ph-CH=N-TEMPO.[2]

The pressure dependence of the magnetic properties of $[Mn(hfac)_2] \cdot (Br\text{-}BNO)$ is studied. The pressure dependence the transition temperature (T_C or T_N) is shown in Figure 5-4-1. The phase diagram of $[Mn(hfac)_2] \cdot (Br\text{-}BNO)$ is divided by three regions.

Figure 5-4-1 The pressure dependence of the critical temperatures (T_N or T_C).

In the pressure region of $p = 0 \sim 3.0$ kbar, the magnetism is a ferrimagnetism. In the pressure region of $p = 3.5 \sim 6.0$ kbar, the magnetic behavior is a metamagnetism. The metamagnetic transition temperature, T_N, becomes higher with increasing

temperature. In the pressure region of $p = 6.0 \sim 8.0$ kbar, the magnetic behavior is also metamagnetism, as well as the region of $p = 3.5 \sim 6.0$ kbar. But T_N is suddenly lowered.

In the ferrimagnetic region, T_C is enhanced, but saturation rate of the magnetization curve becomes slower than the one at ambient pressure. This is related to the enhancement of the antiferromagnetic interaction. In the metamagnetic region below 6.0 kbar, the pressure dependences of T_N and H_C are also related to the enhancement of the antiferromagnetic interaction. This situation is a contrast to the interchain antiferromagnetic interactions in $[\text{Mn(hfac)}_2] \cdot (\text{BNO})$ and $[\text{Mn(hfac)}_2] \cdot (\text{F-BNO})$. The pressure-induced crossover between ferromagnetic and antiferromagnetic states of β-p-NPNN is also explained by the changing of the relative values of intermolecular antiferromagnetic interaction.[3]

Above 6.0 kbar, the pressure dependence of T_N is changed. Structural changes at this pressure are suggested. The ground state is still considered as metamagnetism. The crystal structure of the two dimensional metamagnet of $FeCl_2$ is changed above 1.85 kbar, and pressure dependence of T_N is changed.[4]

References.

1) K. Takeda, M. Mito, T. Kawae, M. Takumi, K. Nagata, M. Tamura and M. Kinoshita, *J. Phys. Chem.*, *B102* (**1998**) 671.

2) M. Mito, T. Kawae, M. Hitaka, T. Ishida and T. Nogami, *Chem. Phys. Lett.*, *33* (**2001**) 69.

3) K. Takeda, M. Mito, T. Kawae, H. Deguchi, S. Takagi, M. Okumura, T. Kawakami, K. Yamaguchi and M. Kinoshita, *Chem. Phys. Lett. 308* (**1999**) 181-186.

4) (a) C. Vettier and E. B. Yellon, *Phys. Rev., B11* (**1975**) 4700, (b) A. Liowsski and Z. Oryszkiewicz, *Phys. Stat. Sol. (b) 131* (**1985**) K117.

$6.$ Pressure Effect in a Ferrimagnet, [Mn(hfac)$_2$]·(Cl-BNO)

K. Suzuki, Y. Hosokoshi and K. Inoue, " Pressure Effects on Molecular Magnets of Mn Complexes with Bisaminoxylbenzene Derivatives", *Mol. Cryst. Liquid. Cryst.*,379 (**2002**) 247-252.

## 6-1. Magnetic Properties in the Pressure Region of $p = 0 \sim 4.0$ kbar

Figure 6-1-1 shows the field dependence of magnetization curves at 2.0 K in the pressure region up to 2.7 kbar. At ambient pressure, magnetizations showed rapid increase below *ca*. 500 Oe and saturated with increasing field due to the ferrimagnetism. In the pressure region below 2.5 kbar, the field dependence of magnetization also showed a rapid increase with increasing field, but the saturation value under low field of magnetization became smaller than the one at ambient pressure. At 2.7 kbar, the form of the magnetization curve changed. The bend of the magnetization curve is noticeable. This bending is related to the spin flip behavior in a metamagnetic behavior. This result means that the magnetic behavior is changed to metamagnetic above $p = 2.7$ kbar, as well as the case of [Mn(hfac)$_2$]·(Br-BNO).
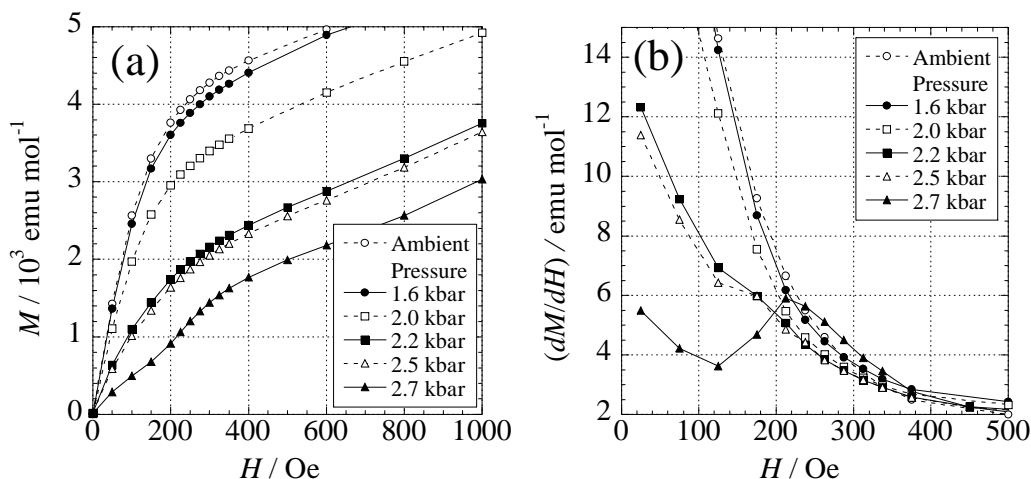
Figure 6-1-1 (a) Field dependence of magnetization (*M*) under several pressures ($p \leq$ 2.7 kbar) at 2.0 K. (b) Field derivatives of magnetizations against field.

Field dependence of magnetization under 2.7 kbar at several temperatures is shown in Figure 6-1-2. At 1.8 K, the spin flip behavior at 200 Oe was noticeable.

Below 5.0 K, magnetization increased rapidly below 100 Oe, and the curvature was changed above 100 Oe. The bends in magnetization curves are recognized as the maxima in the plot of the field derivatives of magnetization field, dM/dH. This spin flip behavior is noticeable below 5.0 K. This result is suggested that the transition temperature of metamagnetism under this pressure is estimated at 5.0 K.
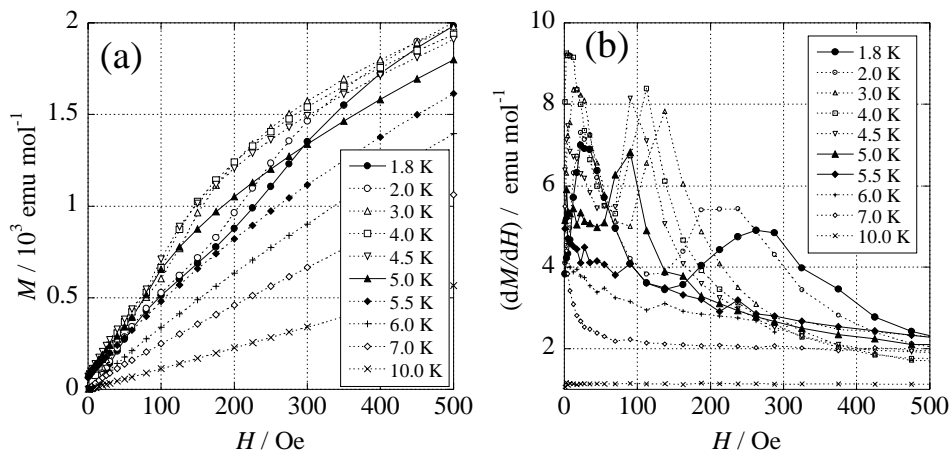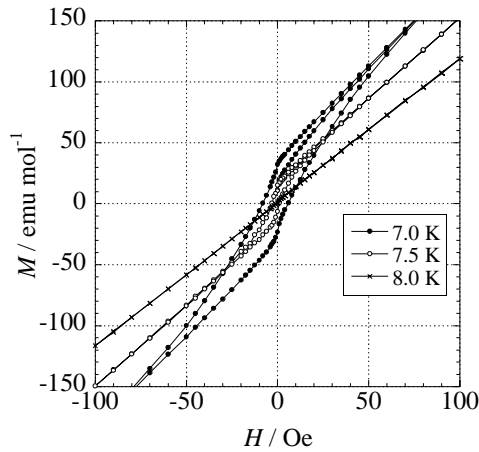

Figure 6-1-2 (a) Temperature dependence of magnetization curves under 2.7 kbar and (b) field derivatives of magnetizations against field.

The temperature dependence of ac susceptibility (χ_{ac}) in the pressure region of $p = 0 \sim 2.7$ kbar is shown in Figure 6-1-3. At ambient pressure, χ' showed an abrupt increased at $T_C = 4.8$ K, and χ'' appeared below this temperature, and increased with decreasing temperature. At 1.6 kbar, χ_{ac} behavior was almost identical with that at ambient pressure. At 2.0 kbar, χ_{ac} behavior was also similar to that at ambient pressure, but a broad shoulder at around 7.5 K was shown in χ''. At 2.5 kbar, χ' showed a peak at 4.2 K and a broad shoulder at around 7.5 K. At 2.7 kbar, χ' showed a peak at 4.2 K accompanied by a shoulder at 5.2 K, and the broad shoulder at around 7.5 K became smaller, but still remained. Figure 6-1-4 shows the magnetization curve at low field

region under 2.2 kbar. Below 7.5 K at which χ' and χ'' made a broad peak, a hysteresis

loop were observed. The existence of ferromagnetic portion is suggested, but the amount

is very small (M_{sat} = 30 emu/mol). We can conclude that the anomaly at around 7.5 K is

related to the contamination of ferromagnetic portion.
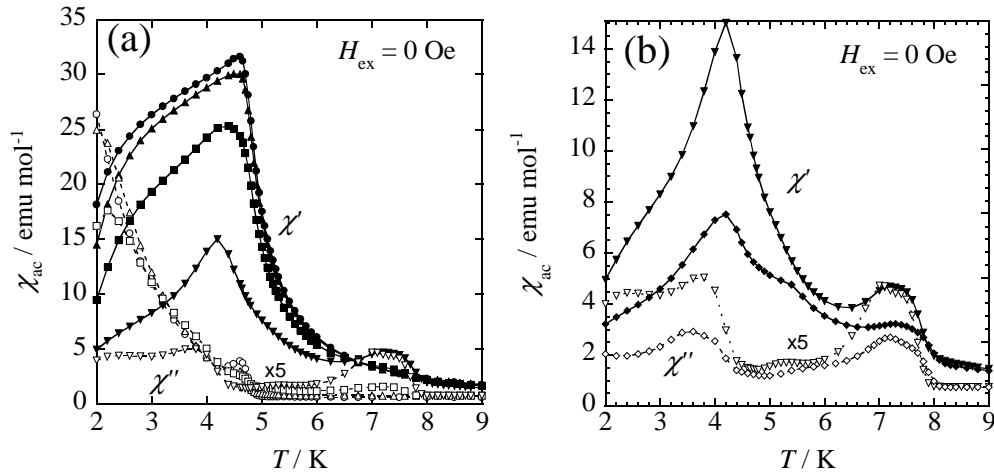
Figure 6-1-3 Temperature dependence χ_{ac}. (a) χ' (full line) at ambient pressure (●) and under 1.6 (▲), 2.0 (■) and 2.5 kbar (▼), and χ'' (dashed line) at ambient pressure (○) and under 1.6 (△), 2.0 (□) and 2.5 kbar (▽). (b) χ' (full line) under 2.5 (▼) and 2.7 kbar (◆), and χ'' (dashed line) under 2.5 (▽) and 2.7 kbar (◇).

**Figure 6-1-4** Magnetization curves at 7.0 (●), 7.5(○) and 8.0 K (×), under 2.2 kbar.

Figure 6-1-5 shows the temperature dependence of χ_{ac} in the several frequency ac fields ($f_{ac} = 1 \sim 500$ Hz). In the all frequency region, the appearing temperatures of χ'' are the almost same. Therefore, this broad shoulder is not related to a spin grass behavior. The origin of this ferromagnetic portion is probably related to the formation of the ferro/ferrimagnetic domains.
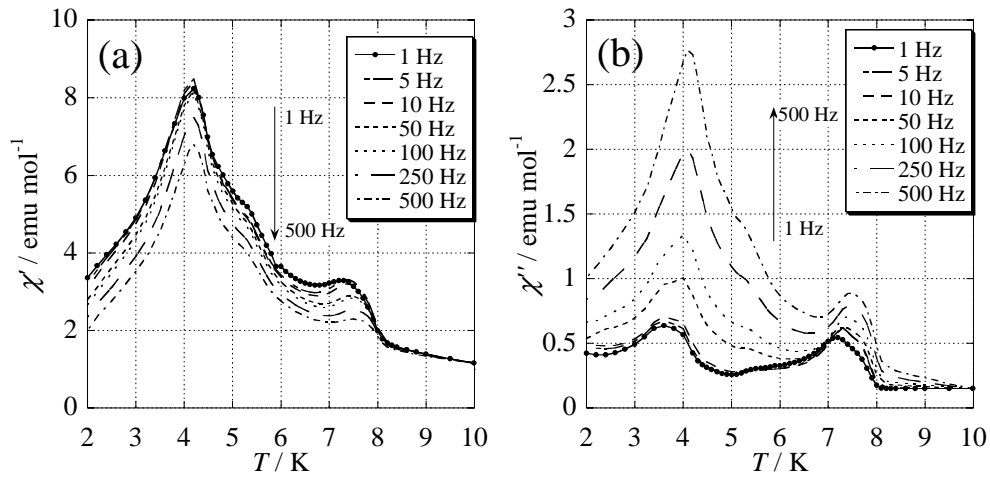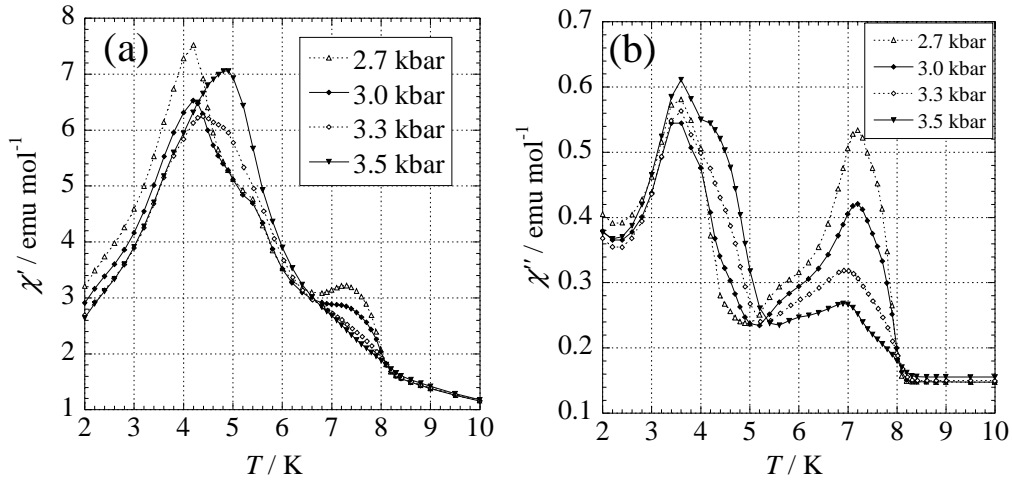

Figure 6-1-5 Temperature dependence χ_{ac} in the several frequency ac fields.(a) χ' and (b) χ''.

When we apply external static fields, the behavior of χ_{ac} is simplified. As is shown in Figure 6-1-6, temperature dependence of χ_{ac} under the external field of 80 Oe showed a sharp peak at 5.0 K. This peak was shifted to lower temperature with increasing field up to 160 Oe. The temperature of the peak of χ' under 80 Oe is consistent with the transition temperature that is estimated from the temperature dependence of H_C. It is related to the transition temperature of metamagnetism under 2.7 kbar. The external field of 80 Oe applied, is enough to saturate the ferromagnetic portion and weaker than H_C.
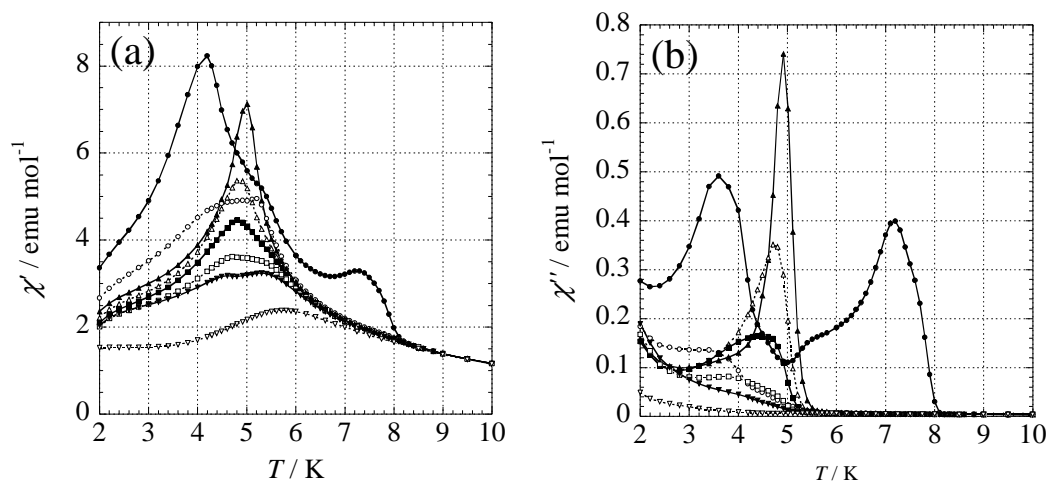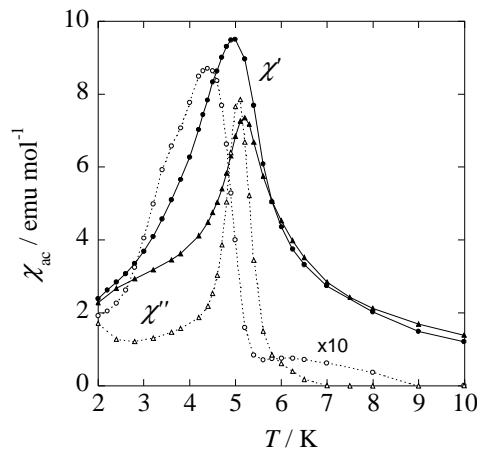
Figure 6-1-6 Temperature dependence of χ_{ac} under 2.7 kbar, under several external static field; $H_{ex} = 0(\bullet)$, $50(\bigcirc)$, $80(\blacktriangle)$, $100(\triangle)$, $120(\blacksquare)$ $160(\square)$, $200(\blacktriangledown)$ and 500 Oe$(\triangledown)$. (a) χ' and (b) χ''

Figure 6-1-7 shows the pressure dependence of χ_{ac} under $H_{ex} = 0$ Oe in the pressure region of $p = 2.7 \sim 3.5$ kbar. When we apply pressure, the behavior of χ_{ac} is simplified. With increasing pressure, the round peaks of χ' and χ'' at around 7.5 K became smaller. Simultaneously, a peak of χ' at 4.2 K under 2.7 kbar was shifted to higher temperature. At 3.5 kbar, χ' showed a peak at 4.9 K. This is a near temperature with T_N. The peak at 3.5 kbar is related the metamagnetic behavior.
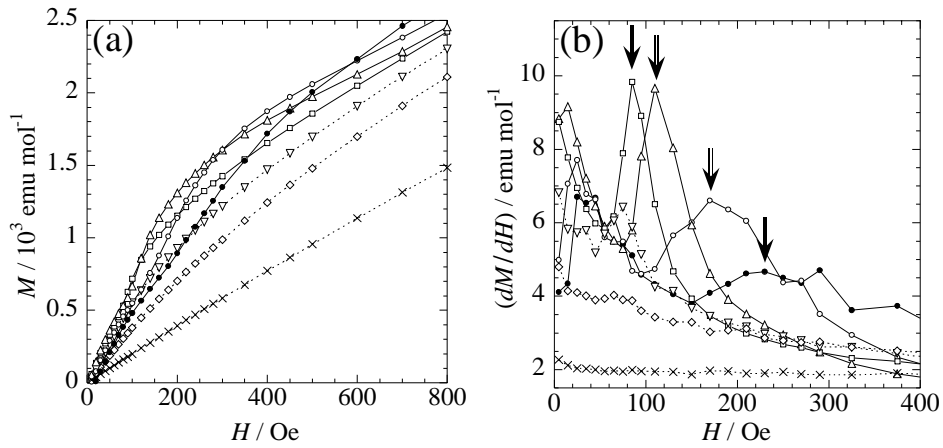

Figure 6-1-7 Temperature dependence of χ_{ac} at ambient pressure ($\bullet$) and under 1.6 ($\bigcirc$), 2.0 ($\blacksquare$), 2.2 ($\square$), 2.5 ($\blacktriangle$), 2.7 ($\triangle$), 3.0 ($\blacklozenge$), 3.3 ($\lozenge$) and 3.5 kbar ($\blacktriangledown$). (a), (b) χ' and (c), (d) χ''.

Figure 6-1-8 shows the temperature dependence of χ_{ac} under 4.0 kbar. χ' made a peak at 5.0 K. χ'' showed the anomaly at around 7.5 K, but χ' had no anomaly at this temperature. The spin flip behavior is noticeable below 5.0 K, at which χ' made a peak (Figure 6-1-9). Therefore, the peak of χ' is related to T_N.
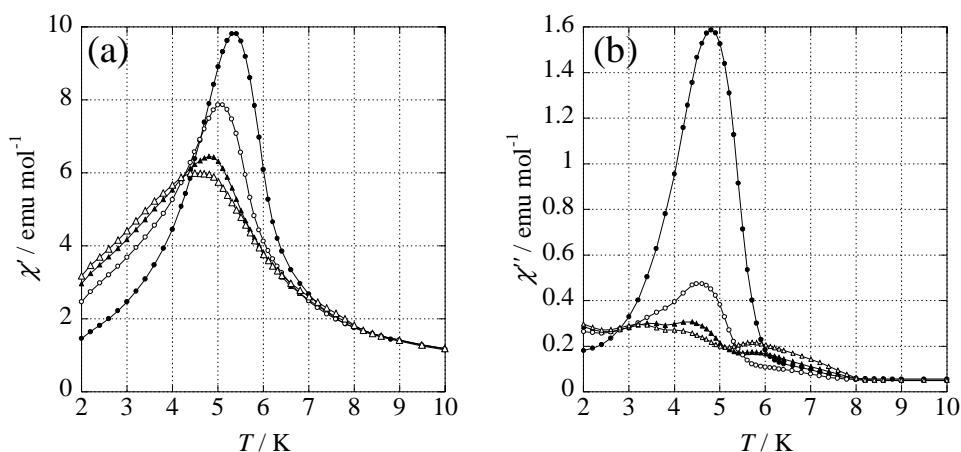

Figure 6-1-8 Temperature dependence of χ_{ac} under 4.0 kbar. χ_{ac} and χ_{ac} under $H_{ex} = 0(\chi';\bullet, \chi'';\circ)$ and 80 Oe($\chi';\blacktriangle$, $\chi'';\triangle$).

Figure 6-1-9 (a) Magnetization curves and (b) dM/dH against field at 4 kbar: 1.8 ($\bullet$), 2.5 ($\circ$), 4.0($\triangle$), 5.0($\square$), 5.5($\triangledown$), 6.0 ($\diamond$) and 7.5 K ($\times$).

6-2. Magnetic Properties in the Pressure Region of $p = 4.0 \sim 7.0$ kbar

Above 4 kbar, the metamagnetic behavior was noticeable in the temperature dependence of χ_{ac}. Figure 6-2-1 shows χ_{ac} in the pressure region of $p = 3.8 \sim 7.0$ kbar. The continuous change of χ_{ac} is observed with increasing pressure. Therefore, the magnetic behavior in this pressure region is related to the metamagnetism as well as the one under $p = 2.7 \sim 4.0$ kbar, and the temperature of the peak is related to T_N. The peak of χ' was shifted to higher temperature with increasing pressure.
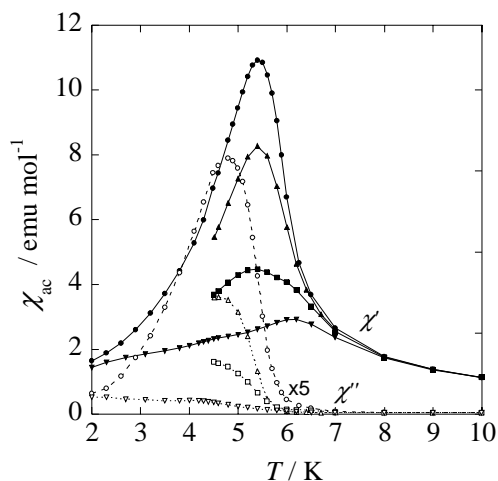

Figure 6-2-1 The temperature dependence of χ_{ac} under 3.8($\triangle$), 4($\blacktriangle$), 5($\bigcirc$) and 7 kbar ($\bullet$). (a) χ' and (b) χ''.

The pressure dependences of magnetization isotherms are shown in Figure 6-2-2. At 2.7 kbar, the spin flip behavior was noticeable under 200 Oe. With increasing pressure, this behavior became weaker. At 7.0 kbar, spin flip behavior was almost disappeared. The reason of this pressure dependence in not known.
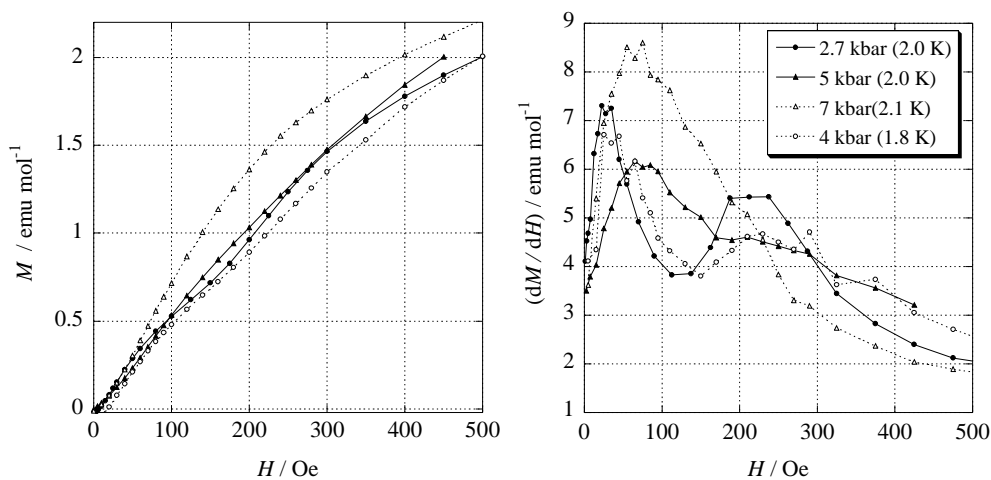
Figure 6-2-2 The field derivatives of magnetizations against field, under 2.7(●), 4.0 (○), 5.0(▲) and 7.0 kbar (△).

Figure 6-2-3 shows the field dependence of χ_{ac} under 7 kbar. Under 0 Oe, χ_{ac} made a peak at 5.4 K. With increasing pressure up to 100 Oe, the peak of χ' reduced and the peak temperature hardly changed.

Figure 6-2-3 Temperature dependence of χ_{ac} at ambient pressure and under 7.0 kbar. χ' and χ'' under $H_{ex} = 0(●, ○)$, 25(▲, △), 100(■, □) and 200 Oe (▼, ▽), respectively.

6-3. Magnetic Properties in the Pressure Region in $p = 7.0 \sim 11.5$ kbar

Temperature dependence of χ_{ac} in the pressure region of $p = 7.0 \sim 11.5$ kbar is shown in Figure 6-3-1. In the pressure region of p = 7.0 ~ 9.5 kbar, c' made a peak that is related to T_N, and this peak is shifted to higher temperature with increasing pressure. Above 10.5 kbar, the shape of χ_{ac} was broadened and complicated. Therefore, χ_{ac} under several fields measured for simplification of χ_{ac} behavior.
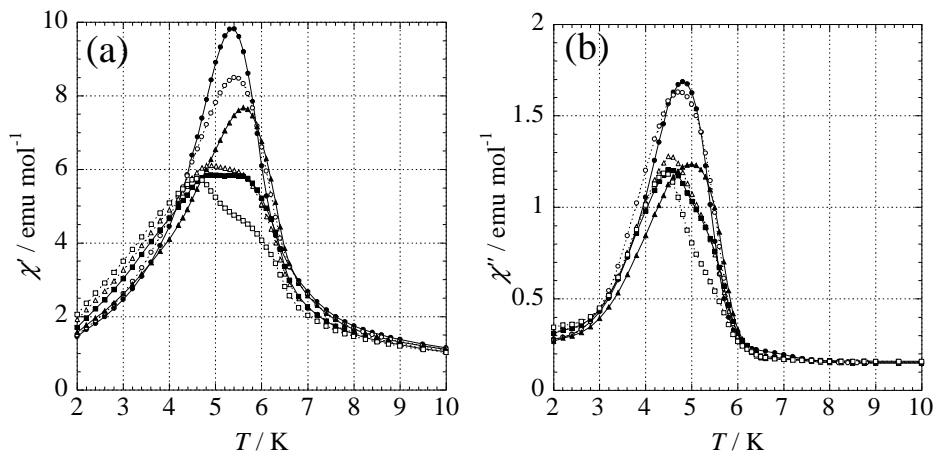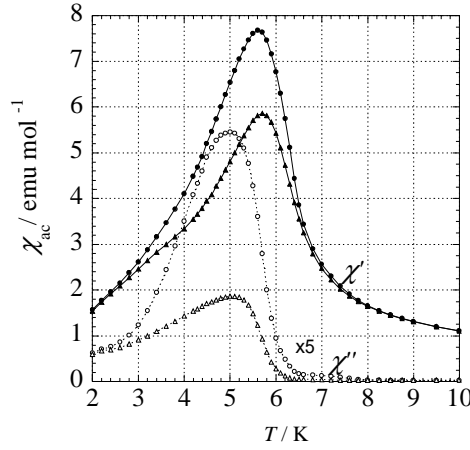

Figure 6-3-1 Temperature dependence of χ_{ac} under 7(●), 9(○), 9.5(▲), 10.5(△), 11(■), 11.5 kbar (□). (a) χ' and (b) χ''.

Temperature dependences of χ_{ac} under 9 and 9.5 kbar in the several pressures are shown in Figures 6-3-2 and 6-3-3, respectively. Under $H_{ex} = 0$, each of χ_{ac} made peak at 5.4 and 5.6 K, respectively. With increasing field, the peak of χ' was shifted to higher temperature.
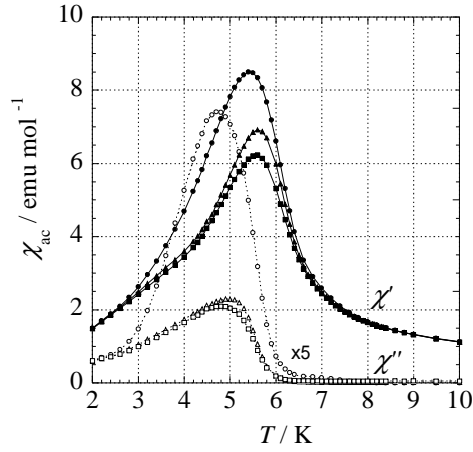
Figure 6-3-2 Temperature dependence of ac susceptibility (χ_{ac}) at 9.0 kbar. The real part of $\chi_{ac}(\chi')$, and the imaginary part of $\chi_{ac}(\chi'')$ under $H_{ex} = 0(\chi'; \bullet, \chi''; \bigcirc)$, 10 ($\chi'; \blacktriangle, \chi''; \triangle$) and 25 Oe ($\chi'; \blacksquare, \chi''; \square$).
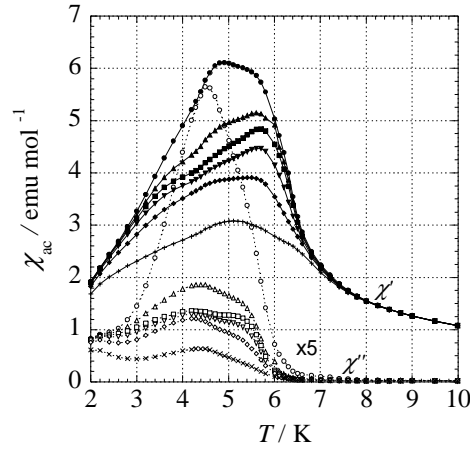

Figure 6-3-3 Temperature dependence of χ_{ac} at 9.5 kbar, under $H_{ex} = 0(\chi'; \bullet, \chi''; \bigcirc)$, 10 ($\chi'; \blacktriangle, \chi''; \triangle$) and 25 Oe ($\chi'; \blacksquare, \chi''; \square$).

The temperature dependences of χ_{ac} under 10.5 kbar in the field region of $H_{ex} = 0 \sim 100$ Oe is shown in Figures 6-3-4. Under $H_{ex} = 0$ Oe, χ' make a broad peak. Under 5 Oe, χ' takes a maximum at around 5.5 K and a shoulder at around 4.7 K. With increasing pressure, the peak at around 5.5 K showed smaller field dependence than the shoulder at around 4.7 K. Therefore, it appears that the main peak of χ' in this pressure is at around 5.5 K, and this temperature defined as T_N. However, the valuations of reduction from field of the peak and the shoulder are similar. Probably, the shoulder is also due to the

metamagnetic behavior.

Figure 6-3-4 Temperature dependence of χ_{ac} at 10.5 kbar. χ' and χ'' under $H_{ex} = 0(\chi';\bullet,$ $\chi'';\bigcirc$), 5 ($\chi';\blacktriangle, \chi'';\triangle$) and 10 Oe ($\chi';\blacksquare, \chi'';\square$), 25($\chi';\blacklozenge, \chi''; \lozenge$), 50($\chi';\blacktriangledown, \chi''; \triangledown$) and 100 Oe($\chi';+, \chi''; \times$).

The temperature dependences of χ_{ac} under 11.5 kbar in the field region of $H_{ex} =$ 0 ~ 100 Oe is shown in Figures 6-3-5. Under $H_{ex} = 0$ Oe, χ' takes a maximum at 4.5 K and a shoulder at around 5.8 K. From the results of the field dependence of the peak of χ', the main peak of χ' in this pressure is estimated at around 4.5 K, and this temperature defined as T_N. However, the shoulder at around 5.8 K is also suggested a metamagnetic portion. This behavior is probably understood as the mixture of some of the metamagnetic portions.
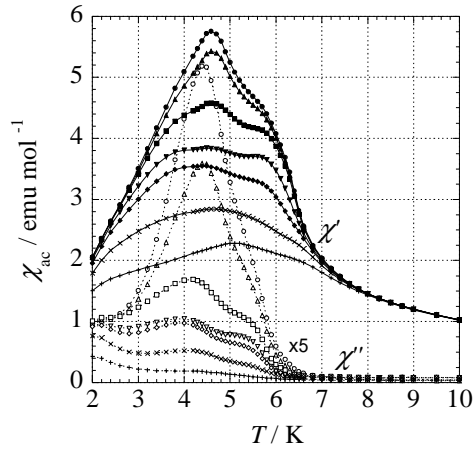
Figure 6-3-5 Temperature dependence of χ_{ac} at 11.5 kbar, under $H_{ex} = 0(\chi'; \bullet, \chi''; \circ)$, 2 $(\chi'; \blacktriangle, \chi''; \triangle)$, 5 Oe $(\chi'; \blacksquare, \chi''; \square)$, 25$(\chi'; \blacklozenge, \chi''; \lozenge)$ 50$(\chi'; \blacktriangledown, \chi''; \triangledown)$, 100$(\chi'; \times, \chi''; \times)$ and 200 Oe$(\chi'; +, \chi''; +)$.

Field dependence of magnetization in the present pressure region is shown in Figure 6-3-6. The S-shape curves were noticeable in the all pressure region. This behavior is related to the spin flip behavior. But, it is not understood that this behavior is due to the same origin with the ones under p = 2.7 and 4.0 kbar, because H_C shows the discontinuous pressure dependency in the metamagnetic region.
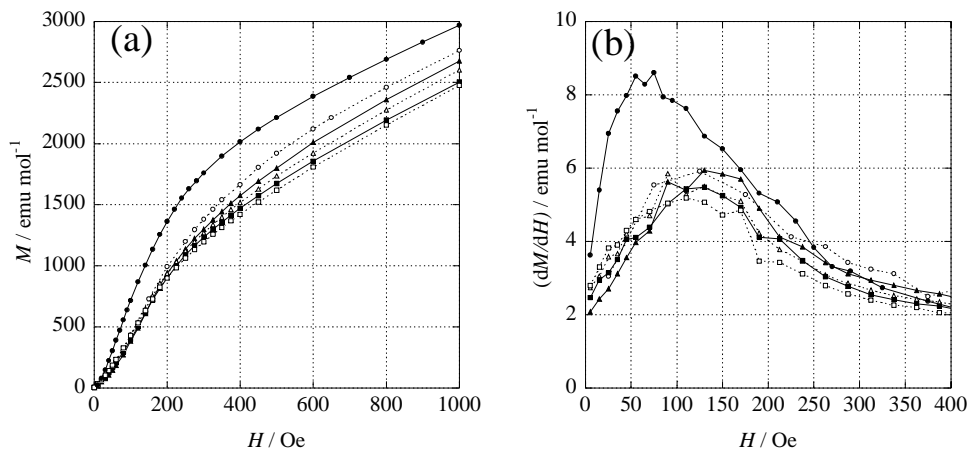
Figure 6-3-6 Field dependence of magnetization up to (a) 1 T and (b)1000 Oe, and (b)(c) field derivatives of magnetizations against field at 2.0 K, under 7($\bullet$; 2.1 K), 9($\circ$), 9.5($\blacktriangle$), 10.5($\triangle$), 11($\blacksquare$), 11.5 kbar ($\square$)

Field dependence of magnetization curve under 11.5 kbar at the several temperatures is shown in Figure 6-3-7. At 4.0 K, the magnetization rate shows the maximum. But dM/dH showed the convex curve up to 5.0 K. The transition temperature is not cleared from the magnetization curves. It related to some peaks of χ'.
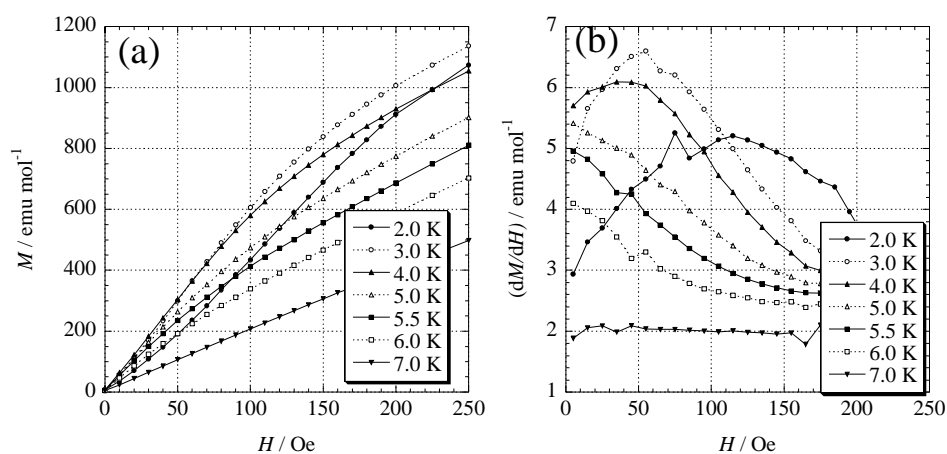
Figure 6-3-7 (a) Field dependence of magnetization and (b) field derivatives of magnetizations against field under 11.5 kbar.

6-4 Conclusion

The pressure dependence of the magnetic properties of $[Mn(hfac)_2]\cdot(Cl\text{-}BNO)$ is studied. The pressure dependence the transition temperature (T_C or T_N) is shown in Figure 6-4-1. The phase diagram of $[Mn(hfac)_2]\cdot(Cl\text{-}BNO)$ is divided by three region, as well as the case of $[Mn(hfac)_2]\cdot(Br\text{-}BNO)$.
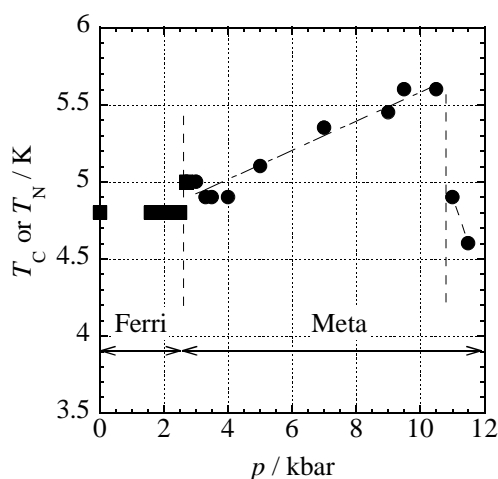
Figure 6-4-1 The pressure dependence of the transition temperature (T_C and T_N)

In the pressure region of $p = 0 \sim 2.7$ kbar, the magnetism is the ferrimagnetism. T_C is hardly changed with increasing pressure. Above 2.7 kbar, the magnetism is changed to the metamagnetism from the ferrimagnetism. The transition temperature of metamagnetism becomes higher with increasing pressure up to 9.5 kbar. This situation is a contrast to the interchain antiferromagnetic interactions in $[Mn(hfac)_2]\cdot(BNO)$ and $[Mn(hfac)_2]\cdot(F\text{-}BNO)$. Above 9.5 kbar, the transition temperature is suddenly lowered. Structural change at this pressure is suggested. The ground state is still considered as metamagnetism. The observed phenomena is understood by the phase diagram similar

73

to the one for [Mn(hfac)$_2$]·(Cl-BNO) The critical pressures are different. It is related to the different between the molecular structures of [Mn(hfac)$_2$]·(Cl-BNO) and [Mn(hfac)$_2$]·(Br-BNO). Their crystal structures are very similar, but the fine structure is probably different. The interchain interactions observe a highly structural dependence. For example, the critical temperatures of them at ambient pressure are different. And the effects of the chemical pressure due to the different in the halogen atoms between the two complexes are also expected.

7. Concluding Remarks

In this thesis, the pressure dependences of the magnetic properties of the four kinds of quasi-one dimensional magnets were investigated.

In Chapter 2, the techniques of magnetic measurements under high pressure are described. We must take care of the effect on eddy current on the metal surface of the pressure clamp cell for the measurements of ac susceptibilities. The low frequency of 1 Hz as ac fields does not affect the measurements. With increasing field, the measurement values from the cell become larger compared with the measurement value from a sample. But measured values of the cells are independent of temperature in the temperature region of $T = 2.0 \sim 10$ K. The measurement of ac susceptibility with high pressure cell can measured in ac field with high frequency up to 500 Oe by subtracting the constant value.

In Chapter 4, the investigations on the pressure dependences of magnetic properties of quasi-one-dimensional metamagnets of $[Mn(hfac)_2]\cdot(BNO)$ and $[Mn(hfac)_2]\cdot(F\text{-}BNO)$ are described. The metamagnetic behaviors are observed up to 11 kbar and the transition temperatures of the metamagnetism and the critical fields of the spin flip behavior become larger with the increasing pressure. This behaviors are suggested the monotonously enhancement of the interchain interaction due to the reducing of the interchain distances.

In Chapters 5 and 6, the investigations on the pressure dependence of magnetic properties of the quasi-one-dimensional ferrimagnets of $[Mn(hfac)_2]\cdot(Br\text{-}BNO)$ and $[Mn(hfac)_2]\cdot(Cl\text{-}BNO)$ are described. The pressure-induced crossovers between ferrimagnetic and metamagnetic stats are observed at the critical fields of $p = 3.5$ (X = Br) and 2.7 kbar (X = Cl), respectively. There still remain traces of ferro/ferrimagnetic domains. The phase diagrams of them are divided by three regions according to the

pressure dependences of transition temperatures (T_C or T_N), as is shown in Figure 7-1. The pressure dependences of T_N of the metamagnetisms become higher with increasing pressure up to 6.0 (X = Br) and 9.5 kbar (X = Cl), respectively. The pressure dependences of magnetic properties up to these pressures, including the ferrimagnetic region, are explained by the enhancement of the interchain antiferromagnetic interaction. This situation is a contrast to the interchain antiferromagnetic interactions in [Mn(hfac)$_2$] ·(BNO) and [Mn(hfac)$_2$]·(F-BNO). Above p = 6.0 (X = Br) and 9.5 kbar (X = Cl), T_N are suddenly lowered. Structural changes at this pressure are suggested. The ground state is still considered as metamagnetism.

Pressure / kbar	1	2	3	4	5	6	7	8	9	10	11~
X = H and F	Metamagnet										
X = Cl	Ferrimagnet		Metamagnet I							Metamagnet II	
X = Br	Ferrimagnet		Metamagnet I		Metamagnet II						

Figure 7-1 The pressure dependences of the magnetic behavior of the four complexes.

Pressurization of the metamagnetic complexes of [Mn(hfac)$_2$]·(BNO) and [Mn(hfac)$_2$]·(F-BNO), yields monotonously enhancement of the interchain interaction as increasing pressure. On the other hand, the ferrimagnetic complexes of [Mn(hfac)$_2$]· (Cl-BNO) and [Mn(hfac)$_2$]·(Br-BNO), show the metamagnetic behavior under pressure. It is suggested that the ferromagnetic interactions appear only for the special condition of molecular overlap, and are readily transformed into antiferromagnetic ones. Since the pressure dependence behaviors are continuously ones up to the limit between the regions of "Metamagnet I" and "Metamagnet II", the phase transitions of the crystal structure are not occurred up to this limit. It appears that the pressure-induced

crossovers of the ferrimagnetic complexes are due to the subtle changing of the ferrimagnetic chain as increasing pressure.

Acknowledgments

Kentaro Suzuki